Face Gear Drive With Spur Involute Pinion: Geometry, Generation by a Worm, Stress Analysis

Faydor L. Litvin, Alfonso Fuentes, Claudio Zanzi, and Matteo Pontiggia
University of Illinois at Chicago, Chicago, Illinois

20020304 092

Since its founding, NASA has been dedicated to the advancement of aeronautics and space science. The NASA Scientific and Technical Information (STI) Program Office plays a key part in helping NASA maintain this important role.

The NASA STI Program Office is operated by Langley Research Center, the Lead Center for NASA's scientific and technical information. The NASA STI Program Office provides access to the NASA STI Database, the largest collection of aeronautical and space science STI in the world. The Program Office is also NASA's institutional mechanism for disseminating the results of its research and development activities. These results are published by NASA in the NASA STI Report Series, which includes the following report types:

- TECHNICAL PUBLICATION. Reports of completed research or a major significant phase of research that present the results of NASA programs and include extensive data or theoretical analysis. Includes compilations of significant scientific and technical data and information deemed to be of continuing reference value. NASA's counterpart of peer-reviewed formal professional papers but has less stringent limitations on manuscript length and extent of graphic presentations.

- TECHNICAL MEMORANDUM. Scientific and technical findings that are preliminary or of specialized interest, e.g., quick release reports, working papers, and bibliographies that contain minimal annotation. Does not contain extensive analysis.

- CONTRACTOR REPORT. Scientific and technical findings by NASA-sponsored contractors and grantees.

- CONFERENCE PUBLICATION. Collected papers from scientific and technical conferences, symposia, seminars, or other meetings sponsored or cosponsored by NASA.

- SPECIAL PUBLICATION. Scientific, technical, or historical information from NASA programs, projects, and missions, often concerned with subjects having substantial public interest.

- TECHNICAL TRANSLATION. English-language translations of foreign scientific and technical material pertinent to NASA's mission.

Specialized services that complement the STI Program Office's diverse offerings include creating custom thesauri, building customized data bases, organizing and publishing research results . . . even providing videos.

For more information about the NASA STI Program Office, see the following:

- Access the NASA STI Program Home Page at *http://www.sti.nasa.gov*

- E-mail your question via the Internet to help@sti.nasa.gov

- Fax your question to the NASA Access Help Desk at 301–621–0134

- Telephone the NASA Access Help Desk at 301–621–0390

- Write to:
  NASA Access Help Desk
  NASA Center for AeroSpace Information
  7121 Standard Drive
  Hanover, MD 21076

Face Gear Drive With Spur Involute Pinion: Geometry, Generation by a Worm, Stress Analysis

Faydor L. Litvin, Alfonso Fuentes, Claudio Zanzi, and Matteo Pontiggia
University of Illinois at Chicago, Chicago, Illinois

National Aeronautics and
Space Administration

Glenn Research Center

February 2002

Acknowledgments

Available from

NASA Center for Aerospace Information
7121 Standard Drive
Hanover, MD 21076

National Technical Information Service
5285 Port Royal Road
Springfield, VA 22100

Available electronically at http://gltrs.grc.nasa.gov/GLTRS

Face Gear Drive with Spur Involute Pinion: Geometry, Generation by a Worm, Stress Analysis

Faydor L. Litvin, Alfonso Fuentes, Claudio Zanzi, Matteo Pontiggia
Gear Research Center, Department of Mechanical Engineering
University of Illinois at Chicago
Chicago, Illinois 60607

Abstract

A face gear drive with a spur involute pinion is considered. The generation of the face gear is based on application of a grinding or cutting worm whereas the conventional method of generation is based on application of an involute shaper. An analytical approach for determination of: (i) the worm thread surface, (ii) avoidance of singularities of the worm thread surface, (iii) dressing of the worm, and (iv) determination of stresses of the face-gear drive, is proposed. A computer program for simulation of meshing and contact of the pinion and face-gear has been developed. Correction of machine-tool settings is proposed for reduction of the shift of the bearing contact caused by misalignment. An automatic development of the model of five contacting teeth has been proposed for stress analysis. Numerical examples for illustration of the developed theory are provided.

Nomenclature

α_c	Pressure angle for symmetric face-gear drive for driving and coast sides
$\Delta\gamma$	Change of shaft angle
ΔE	Change of shortest distance between the pinion and the face-gear axes
Δq	Axial displacement of face gear
λ_w	Crossing angle between axes of shaper and worm
γ_m	Shaft angle
η_s	Half of the width of the space on the base cylinder
$\Sigma_i \, (i = s, 1, 2, w)$	Tooth surface of the shaper $(i = s)$, of the pinion $(i = 1)$, of the face-gear $(i = 2)$, of the generating worm $(i = w)$
$\psi_i \, (i = s, 2, w)$	Angle of rotation of the shaper $(i = s)$, of the face gear $(i = 2)$ and of the worm $(i = w)$ applied for the process of generation
θ_s, u_s	Surface parameters

E_{sw} Shortest distance between the axes of the shaper and the worm

$L_i = (i = 1,2)$ Inner $(i = 1)$ and outer $(i = 2)$ limiting dimensions of the face gear

l_w Translational motion of the worm in the process of the generation of the face-gear

$\mathbf{M}_{ji}, \mathbf{L}_{ji}$ Matrices 4×4 and 3×3 for transformation from S_i to S_j of point coordinates and projections of vectors

$N_i(i = s,1,2,w)$ Number of teeth of the shaper $(i = s)$, of the pinion $(i = 1)$, of the face-gear $(i = 2)$, of the generating worm $(i = w)$

P_d Diametral pitch

r_{ps} Radius of the pitch circle of the shaper

r_{p1} Radius of the pitch circle of the pinion

r_{bs} Radius of the base cylinder

1. Introduction

A face gear drive with intersected axes formed by a spur pinion and conjugated face gear is considered. The advantages of application of face gear drives in helicopter transmissions (Fig.1) are the possibility of the split of the torque and reduction of weight. The existing design of face gear drives is based on application of an involute spur pinion of the drive. A substantial step in the technology of face-gear drives is the development of grinding (and hobbing) of face gears by a grinding worm (a hob, respectively) [14].

The contents of the paper cover:

(1) A brief summary of the existing geometry and output of TCA (Tooth Contact Analysis) computer program developed for simulation of meshing and contact.

(2) Concept of generation of face-gears by grinding or cutting worm, analytical derivation of worm thread surface, its dressing and avoidance of undercutting of the worm generated by the shaper.

(3) Stress analysis of face-gear drives. A model with five contacting teeth is developed automatically.

The performed research is based on application of modern theory of gearing that has been a subject of research by V. A. Zalgaller [21], [22], N. Stosik [18], [19], [20], G. Bar [4], G. I. Shevelova [16], Baummann [3], Stadtfeld [17] and F. L. Litvin and his followers [1], [2], from [7] to [13]. The developed theory is illustrated with numerical examples.

2. Geometry of Existing Design

Generation of Face-Gear. The conventional method of generation of the face-gear is based on application of an involute shaper. The process of generation is based on simulation of meshing of the face-gear with the involute shaper. The authors have considered as well a prospective method for generation of the face-gear by a worm that might be applied as a grinding worm or a hob (section 3).

Localization of Contact. Localization of the bearing contact between the tooth surfaces of the involute pinion and the face gear is achieved as follows:

1. The face-gear may be determined as the envelope to the family of surfaces of an involute shaper with tooth number $N_S > N_p$ where N_S and N_p are the tooth numbers of the shaper and the pinion of the drive. Usually,

   $$N_S - N_p = 2 \Leftrightarrow 3.$$

2. The pinion and the shaper of the drive are in an imaginary internal tangency as shown in Fig. 2.

3. We may consider that three surfaces Σ_S, Σ_2 and Σ_1 are in mesh simultaneously. The surfaces of the shaper Σ_S and the face-gear Σ_2 are in line tangency at every instant. However, surface Σ_2 and pinion surface Σ_1 are in tangency at a point at every instant since $N_p < N_s$.

Structure of Face Gear Tooth. The tooth surfaces Σ_2 of the face-gear generated by an involute shaper are shown in Fig. 3(a). Lines L_{2S} represent the instantaneous lines of tangency of Σ_2 .and shaper Σ_S shown on Σ_2. The cross-sections of the face-gear tooth are shown in Fig. 3(b). Investigation shows that the surface points of the face-gear are hyperbolic ones. This means that the product of principal curvatures at the surface point is negative. The fillet of the face-gear tooth surface of a conventional design (Fig. 3) is generated by the edge of the shaper. The authors have proposed to generate the fillet by a rounded edge of the shaper as shown in Fig. 4 that allows the bending stresses to be reduced approximately in 10%. The shape of the modified fillet of the face gear is shown in Fig. 5.

The length of the face-gear teeth has to be limited by dimensions L_1 and L_2 (Fig. 6) to avoid [8]: (i) undercutting in plane A, and (ii) tooth pointing in plane B. The permissible length of the face-gear tooth is determined by the unit less coefficient c represented as

$$c = (L_2 - L_1)P_d = \frac{L_2 - L_1}{m} \tag{1}$$

where P_d and m are the diametral pitch and the module, respectively. The magnitude of coefficient c depends mainly on the gear ratio $m_{12} = \dfrac{N_2}{N_1}$ and is usually in the range $8 < c < 15$.

Results of TCA (Tooth Contact Analysis). TCA is designated for simulation of meshing and contact of surfaces Σ_1 and Σ_2 and permits the investigation of the influence of errors of alignment on transmission errors and the shift of bearing contact. The TCA algorithm is based on observation of continuous tangency of pinion and face-gear tooth surfaces Σ_1 and Σ_2 (See details in [8]). Application of the TCA program indicates: (i) errors of alignment do not cause transmission errors, but (ii) cause the shift of bearing contact. The advantage of zero transmission errors is the result of application of an involute pinion that has equidistant profiles.

The sensitivity of the bearing contact of the face gear drive to errors of alignment requires special corrections to obtain a central location of the bearing contact. It has been proven that this can be obtained by axial displacement Δ_q of the face-gear with respect to the pinion.

The investigation is based on application of coordinate systems shown in (Figs. 7 and 8). Coordinate systems S_1 and S_f are rigidly connected to the pinion and the frame of the face-gear drive, respectively (Fig. 7(a)). To simulate the misalignment of the face-gear, we use auxiliary coordinate systems S_q (Fig. 7(b)), S_d and S_e (Fig. 8(a)). The location of S_q with respect to S_f is shown in Fig. 7(b). Parameters ΔE, B and $B \cot \gamma$ determine the location of the origin O_q with respect to O_f. Here, ΔE is the shortest distance between the pinion and the face-gear axes when the axes are crossed but not intersected; parameters B and $B \cot \gamma$ are shown in Fig. 7(b).

Auxiliary fixed coordinate systems S_q, S_d and S_e are shown in Fig. 8(a). The face-gear performs rotation about the z_e axis (Fig. 8(b)). The location of S_e with respect to S_d simulates the axial displacement Δq of the face-gear (Fig. 8(b)). The orientation of S_d with respect to S_q simulates the installment of the crossing angle $\gamma = \gamma_m + \Delta \gamma$, where γ_m is the shaft angle, and $\Delta \gamma$ is caused by the misalignment (Fig. 8(a)).

Numerical Example 1.

The output of TCA has been obtained for a face gear drive with the following data:

Pinion tooth number $N_1 = 25$

Face gear tooth number $N_2 = 160$

Shaper tooth number $N_S = 28$

Crossing angle $\gamma_m = 90°$

Pressure angle $\alpha_c = 25°$.

Fig. 9 shows: (i) the bearing contact of aligned gear drive (Fig. 9(a)), and (ii) the shift of bearing contact caused by errors $\Delta\gamma$ and ΔE (Figs. 9(b) and 9(c)). Fig. 10 shows that the location of the bearing contact is restored by axial displacement Δq of the face gear.

3. Application of Generating Worm

Concept of Generating Worm. The conventional method for generation of a face-gear is based on:

(i)   Application of an involute shaper, and

(ii)   Manufacturing of face-gear based on simulation of meshing of the shaper and the face-gear being generated.

Edward W. Miller has proposed in 1942 the generation of the face-gear by a hob [15]. The rational part of his patent was the idea of consideration of internal meshing of the hob with the pinion of the face-gear drive. However, the patent did not provide the necessary conditions of conjugation of the tooth surfaces of the hob, the pinion, and the face-gear, directions of worm design, and avoidance of worm singularities. Therefore, undercutting of the face-gear and impermissible deviations of the face-gear tooth surface from the theoretical one could not be avoided.

The next step was done by the patent proposed by Litvin et al. [14] that has provided the exact determination of the thread surface of a generating worm that might be applied for grinding and cutting of face-gears.

This paper covers the solution to the following problems of the design of a grinding worm:

1.   Determination of crossing angle between the axes of the shaper and the worm

2.   Determination of worm thread surfaces

3.   Avoidance of singularities of the worm thread surface

4.   Dressing of worm thread surface

Crossing Angle Between Axes of Shaper and Worm. Fig. 11 shows fixed coordinate systems S_a, S_b and S_c applied for illustration of installment of the worm with respect to the shaper. Moveable coordinate systems S_s and S_w are rigidly connected to the shaper and the worm. Axis z_s (it coincides with z_a) is the axis of rotation of the

shaper. Axis z_w (it coincides with z_c) is the axis of rotation of the worm. Axes z_s and z_w are crossed and form a crossing angle $90° \pm \lambda_w$. The upper (and lower) sign corresponds to application of a right-hand (left-hand) worm. The shortest distance between axes z_s and z_w is designated as E_{ws}.

The derivation of crossing angle λ_w is based on observation of simultaneous tangency of surfaces Σ_s, Σ_2, Σ_w. For the purpose of simplification of derivations, we consider the tangency of those surfaces that are equidistant to Σ_s, Σ_2 and Σ_w and pass through point P determined in S_a as (Figs. 11 and 12)

$$\mathbf{r}_a^{(P)} = \begin{bmatrix} r_{ps} & 0 & 0 \end{bmatrix}^T \tag{2}$$

where r_{ps} is the radius of the pitch circle of the shaper.

The derivation of crossing angle λ_w is based on the following procedure:

Step 1: We consider initially the tangency at P of surfaces that are equidistant to Σ_s and Σ_2. Axes z_s and z_2 of rotation of the shaper and the face-gear are intersected (Fig. 12), and therefore there is an instantaneous axis of rotation $O_s I$ that passes through intersection point O_m [8]. Point P is chosen on $O_m I$. Tangency of surfaces Σ_s and Σ_2 is provided because the normals to Σ_s pass through point P (Figs. 12, 15).

Step 2: Tangency of surfaces Σ_s and Σ_w at point P is observed, if the following equation of meshing between Σ_s and Σ_w is satisfied at P [8].

$$\mathbf{N}^{(s)} . \mathbf{v}^{(sw)} = 0 \tag{3}$$

Here: $\mathbf{N}^{(s)}$ is the normal to Σ_s; vector $\mathbf{v}^{(sw)}$ is determined as $\mathbf{v}^{(sw)} = \mathbf{v}^{(s)} - \mathbf{v}^{(w)}$, where $\mathbf{v}^s$ and $\mathbf{v}^w$ are the velocities of point P of the shaper and the worm.

Using equation (3), we obtain after derivations that

$$\lambda_w = \arcsin \frac{r_{ps}}{N_s (E_{ws} + r_{ps})} \tag{4}$$

Here: r_{ps} is the pitch radius of the shaper, and E_{ws} (Fig. 11) is the shortest distance between the axes of the shaper and the worm. The magnitude of E_{ws} affects the dimensions of the grinding worm and the conditions of avoidance of surface singularities of the worm (see below). The meshing of the worm and the shaper is schematically illustrated in Fig. 13.

Analytical Consideration of Simultaneous Meshing of Surfaces Σ_s, Σ_w and Σ_2.

Designations Σ_s, Σ_w and Σ_2 indicate surfaces of the shaper, worm and face-gear, respectively. Simultaneous meshing of Σ_s, Σ_w and Σ_2 is illustrated by Fig. 14.

Shaper surface Σ_s is considered as a given generating one. Surfaces Σ_w and Σ_2 are generated as the envelopes to the family of a shaper surface Σ_s.

Determination of Σ_w.

Step 1: Shaper surface Σ_s is represented as an involute surface of a spur gear (Fig. 15) determined by the equations

$$\begin{cases} x_s = r_{bs}[\cos(\theta_s + n_s) + \theta_s \sin(\theta_s + n_s)] \\ y_s = r_{bs}[\pm \sin(\theta_s + n_s) \mp \theta_s \cos(\theta_s + \eta_s)] \\ z_s = u_s \end{cases} \tag{5}$$

Here u_s and θ_s are surface parameters; parameter n_s determines half of the width of the space on the base cylinder; r_{bs} is the radius of the base cylinder. Parameters θ_s and n_s are shown in Fig. 15; parameter u_s is directed along the z_s-axis. The upper and lower signs in equation of $y_s(\theta_s)$ correspond to profiles I and II, respectively.

Step 2: The worm surface Σ_w is determined in coordinate system S_w (Fig. 11) by the following equations [8]

$$\mathbf{r}_w(u_s, \theta_s, \psi_s) = \mathbf{M}_{ws}(\psi_s)\mathbf{r}_s(u_s, \theta_s) \tag{6}$$

$$\left(\frac{\partial \mathbf{r}_w}{\partial u_s} \times \frac{\partial \mathbf{r}_w}{\partial \theta_s}\right) \cdot \frac{\partial \mathbf{r}_w}{\partial \psi_s} = f_{ws}(u_s, \theta_s, \psi_s) = 0 \tag{7}$$

Here: vector function $\mathbf{r}_w(u_s, \theta_s, \psi_s)$ is the family of shaper surfaces Σ_s represented in S_w; matrix $\mathbf{M}_{ws}(\psi_s)$ describes coordinate transformation from S_s to S_w; equation (7) is the equation of meshing between Σ_s and Σ_w. Parameters (u_s, θ_s) in vector function $\mathbf{r}_w(u_s, \theta_s, \psi_s)$ represent the surface parameters of the shaper; parameter ψ_s in $\mathbf{r}_w(u_s, \theta_s, \psi_s)$ is the generalized parameter of motion. As a reminder, that during generation of the worm the shaper and the worm perform rotations about crossed axes z_a and z_w (Fig. 11). Angles of rotation ψ_s and ψ_w (Fig. 11) are related by the equation

$$\frac{\psi_s}{\psi_w} = \frac{1}{N_s} \tag{8}$$

where N_s is the number of teeth of the shaper. It is assumed that a one-thread worm is applied. Figure 13 shows a schematic illustration of meshing of the shaper and the worm.

Equation of meshing (7) may be represented as well as [7], [8], [9].

$$\mathbf{N}_s \cdot \mathbf{v}_s^{(sw)} = f_{ws}(u_s, \theta_s, \psi_s) = 0 \tag{9}$$

Vector function $\mathbf{r}_w(u_s, \theta_s, \psi_s)$ and equation of meshing $f_{ws} = (u_s, \theta_s, \psi_s) = 0$ represent the worm thread surface Σ_w by three related parameters. Surface Σ_w may be represented in form of two parameters by using the theorem of implicit function systems existence [6], [21].

Assume that equation of meshing $f_{ws} = 0$ is satisfied at a point $M\left(u_s^{(0)}, \theta_s^{(0)}, \psi_s^{(0)}\right)$ and at this point we have that $\dfrac{\partial f_{ws}}{\partial \theta_s} \neq 0$. Then equation $f_{ws}\left(u_s, \theta_s, \psi_s\right) = 0$ may be solved in the neighborhood of M by a function of class C^1 as

$$\theta_s = \theta_s\left(u_s, \psi_s\right) \tag{10}$$

and the worm thread surface Σ_w may be determined locally as

$$\mathbf{r}_w\left(u_s, \theta_s\left(u_s, \psi_s\right), \psi_s\right) = \mathbf{R}_w\left(u_s, \psi_s\right) \tag{11}$$

Determination of Σ_2

Step 1: The derivation of the face-gear surface Σ_2 is based on the following considerations:

(i)   The shaper and the face-gear perform rotations about intersected axes z_s and z_2 that form angle γ_m in a non-orthogonal face-gear drive (Fig. 12). Rotations of the shaper and face-gear are performed in a fixed coordinate system S_m; z_m is the designation of the axis of rotation of the face-gear (Fig. 12).

(ii)   Face-gear tooth surface Σ_2 is determined in coordinate system S_2 by the following equations

$$\mathbf{r}_2\left(u_s, \theta_s, \psi_s\right) = \mathbf{M}_{2s}\left(\psi_s\right)\mathbf{r}_s\left(u_s, \theta_s\right) \tag{12}$$

$$\left(\frac{\partial \mathbf{r}_2}{\partial u_s} \times \frac{\partial \mathbf{r}_2}{\partial \theta_s}\right) \cdot \frac{\partial \mathbf{r}_2}{\partial \psi_s} = f_{2s}\left(u_s, \theta_s, \psi_s\right) = 0 \tag{13}$$

Here, parameters of vector function $\mathbf{r}_2\left(u_s, \theta_s, \psi_s\right)$ designate surface parameters $\left(u_s, \theta_s\right)$, of the shaper and generalized parameter of motion ψ_s. The angles of rotation of the shaper, ψ_s, and the face-gear, ψ_2, are related as:

$$\frac{\psi_s}{\psi_2} = \frac{N_2}{N_s} \tag{14}$$

where N_s and N_2 are the teeth numbers of the shaper and the face gear, respectively.

Equation (12) represents in coordinate system S_2 the family of shaper surfaces Σ_s. Matrix $\mathbf{M}_{2s}$ provides coordinate transformation from coordinate system S_s to S_2. Equation (13) is the equation of meshing between Σ_s and Σ_2 of the shaper and the face-gear. An alternative form of equation of meshing, similar to equation (9), might be applied as well.

Step 2: It follows from the previous discussions that the shaper surface Σ_s is in line contact with the worm surface Σ_w and the face-gear tooth surface Σ_2. Such type of surface contact is obtained because Σ_w and Σ_2 are generated as

envelope of shaper surface Σ_s. We designate by L_{sw} the line of tangency between Σ_s and Σ_w and by L_{s2} the line of tangency between Σ_s and Σ_2.

Investigation of lines L_{sw} and L_{s2} shows that they do not coincide with each other but are intersected at any position of meshing. Figs. 16(a) and fig16(b) show lines of tangency L_{sw} and L_{s2} that are functions of ψ_s and are represented in plane of parameters (u_s, θ_s). Fig.16(c) shows that lines $L_{sw}\left(\psi_s^{(i)}\right)$ and $L_{s2}\left(\psi_s^{(i)}\right)$ intersect with each other at a position of meshing $\psi_s = \psi_s^{(i)}$. The point of intersection of $L_{sw}\left(\psi_s^{(s)}\right)$ and $L_{s2}\left(\psi_s^{(s)}\right)$ corresponds to the point of tangency of surfaces Σ_w and Σ_2.

Vector function $\mathbf{r}_2\left(u_s, \theta_s, \psi_s\right)$ and equation of meshing (13) represent surface Σ_2 by three related parameters. Using the theorem of implicit function system existence, we may represent the face-gear tooth surface Σ_2 in form of two parameters but locally as it was done for surface Σ_w (see representation of vector equations (11)).

Generation of Surface Σ_2 by Worm Surface Σ_w. Remembering that the shaper surface Σ_s is in line contact with worm surface Σ_w and with face-gear tooth surface Σ_2, however, surfaces Σ_w and Σ_2 are in point contact with each other at any instant. This means that finishing grinding of Σ_2 by worm surface Σ_w cannot be accomplished. A grinding process based on related rotations of the worm and the face-gear will provide on Σ_2 only a strip as the set of points of tangency of Σ_w and Σ_2. Therefore generation of Σ_2 by the worm has to be based on a two-parameter enveloping process whereas two independent sets of parameters are provided as: (i) a set of angles of rotation $\left(\psi_w, \psi_2\right)$ of the worm and the face-gear, and (ii) a translational motion l_w of the worm. Parameters ψ_w and ψ_2 are the angles of rotation of the worm and the face-gear related by the equation:

$$\frac{\psi_w}{\psi_2} = \frac{N_2}{N_w} \tag{15}$$

where N_2 and N_w are the number of teeth of the face-gear and the number of threads of the worm. Usually one-thread of worm is applied and $N_w = 1$.

Parameter l_w of translational motion is provided as collinear to the axis of the shaper (see below).

The following coordinate systems are applied for derivation of the face gear surface:

(i)   Fixed coordinate system S_b and S_c where we consider the rotation of the worm (Figs. 11 and 14)

(ii)   Fixed coordinate system S_m where we consider the rotation of the face-gear (Fig. 12)

(iii)   Movable coordinate system S_w rigidly connected to the worm (Fig. 11) and coordinate system S_2 rigidly connected to the face-gear.

Surface Σ_2 of the face-gear generated by the worm is determined by the following equations [7], [8], [21]:

$$\mathbf{r}_2\left(u_s,\theta_s,\psi_w,l_w\right)=\mathbf{M}_{2w}\left(\psi_w,l_w\right)\mathbf{r}_w\left(u_s,\theta_s\left(u_s,\psi_s\right),\psi_s\right) \qquad (16)$$

$$\left[\left(\frac{\partial\mathbf{r}_2}{\partial u_s}+\frac{\partial\mathbf{r}_2}{\partial\theta_s}\frac{\partial\theta_s}{\partial u_s}\right)\times\left(\frac{\partial\mathbf{r}_2}{\partial\psi_s}+\frac{\partial\mathbf{r}_2}{\partial\theta_s}\frac{\partial\theta_s}{\partial\psi_s}\right)\right]\cdot\frac{\partial\mathbf{r}_2}{\partial\psi_w}=0 \qquad (17)$$

$$\left[\left(\frac{\partial\mathbf{r}_2}{\partial u_s}+\frac{\partial\mathbf{r}_2}{\partial\theta_s}\frac{\partial\theta_s}{\partial u_s}\right)\times\left(\frac{\partial\mathbf{r}_2}{\partial\psi_s}+\frac{\partial\mathbf{r}_2}{\partial\theta_s}\frac{\partial\theta_s}{\partial\psi_s}\right)\right]\cdot\frac{\partial\mathbf{r}_2}{\partial l_w}=0 \qquad (18)$$

Here, vector function

$$\mathbf{r}_w\left(u_s,\theta_s\left(u_s,\psi_s\right),\psi_s\right)=\mathbf{R}_w\left(u_s,\psi_s\right) \qquad (19)$$

represents the worm surface. Function $\theta_s\left(u_s,\psi_s\right)$ is obtained from equation of meshing (7) by using the theorem of implicit function system existence. Matrix $\mathbf{M}_{2w}\left(\psi_w,l_w\right)$ represents the coordinate transformation from S_w to S_2. Vector function $\mathbf{r}_2\left(u_s,\theta_s,\psi_w,l_w\right)$ represents in coordinates system S_2 the family of worm surfaces Σ_w. Equations (17) and (18) represent the two equations of meshing of the two parameter enveloping process of generation. The cross-product of vectors in equations (17) and (18) represents in coordinate system S_2 the normal to the worm surface. Vectors $\dfrac{\partial\mathbf{r}_2}{\partial\psi_w}$ and $\dfrac{\partial\mathbf{r}_2}{\partial l_w}$ are equivalent to the relative velocities for generation of two sets of independent motions.

The generated surface Σ_2 of the face-gear is covered by two families of contact lines I and II that correspond to $l_w\neq\text{const}$, $\psi_w=\text{const}$ (Fig. 17(a)) and $\psi_w\neq\text{const}$, $l_w=\text{const}$ (Fig. 17(b)), respectively. Instantaneous point M of tangency of worm and face-gear tooth surface is the point of intersection of lines I and II (Fig. 17(c)). The derivations performed above have resulted two versions of equations of face-gear tooth surface Σ_2: (i) equations from (16) to (18) that correspond to generation of Σ_2 by the worm, and (ii) equations (12) and (13) that correspond to generation of Σ_2 by the shaper. Certainly, the computation of Σ_2 by the mentioned equations will provide the same numerical results.

Avoidance of Singularities of Worm Thread Surface. The worm thread surface has to be designed as a *regular* one. Surface point M is a singularity one if the surface normal is equal to zero at M. Determination of surface singularities is a complex problem for a surface represented by three related parameters, such as the worm thread surface (see equations (6) and (7)). We use in the upcoming discussions the following designations: Σ_w for the three-parameter surface, and Σ_s for the tool surface that generates Σ_w. Surface Σ_w is the envelope to the family of surfaces Σ_s.

Two alternative approaches for determination of singularities of surface Σ_w might be applied:

(i)   The first one (proposed by Zalgaller [21], [22]) is based on direct determination of normal $\mathbf{N}_w$ to surface Σ_w.

(ii)   The second approach is based on consideration of tool surface Σ_s instead of Σ_w (proposed by Litvin [8]). The main goal of the second approach is to simplify derivations since Σ_s is a two parameter surface. The main idea of the approach is to determine initially those regular points on Σ_s that generate singular points on Σ_w.

The singularity equation in first approach is represented as

$$\left(\frac{\partial \mathbf{r}_w}{\partial \theta_s} \times \frac{\partial \mathbf{r}_w}{\partial \psi_s}\right)\frac{\partial f_{ws}}{\partial u_s} + \left(\frac{\partial \mathbf{r}_w}{\partial \psi_s} \times \frac{\partial \mathbf{r}_w}{\partial u_s}\right)\frac{\partial f_{ws}}{\partial \theta_s} + \left(\frac{\partial \mathbf{r}_w}{\partial u_s} \times \frac{\partial \mathbf{r}_w}{\partial \theta_s}\right)\frac{\partial f_{ws}}{\partial \psi_s} = \mathbf{0} \tag{20}$$

Here, vector function $\mathbf{r}_w\left(u_s,\theta_s,\psi_s\right)$ is determined from equation (6); $f_{ws}\left(u_s,\theta_s,\psi_s\right)=0$ is the equation of meshing (7).

The second approach is based on the following considerations:

(1) It is proven that surface singularity occurs if the following equation is observed [8]

$$\mathbf{v}_r^{(s)} + \mathbf{v}_r^{(sw)} = \mathbf{0} \tag{21}$$

Here: $\mathbf{v}_r^{(s)}$ is the velocity of a point that moves over the tool surface Σ_s; $\mathbf{v}_r^{(sw)}$ is the relative sliding velocity in meshing of surfaces Σ_s and Σ_w. Vectors of equation (21) are represented in coordinate system S_s.

(2) We apply in addition to equation (21) the differentiated equation of meshing (7) of the worm and the shaper. Then we obtain:

$$\frac{\partial f_{ws}}{\partial u_s}\frac{du_s}{dt} + \frac{\partial f_{ws}}{\partial \theta_s}\frac{d\theta_s}{dt} + \frac{\partial f_{ws}}{\partial \psi_s}\frac{d\psi_s}{dt} = 0 \tag{22}$$

(3) Applications of equations (21) and (22) results in a system of four linear equations in two unknowns. The system has a certain solution for the unknowns if the matrix

$$\mathbf{A} = \begin{bmatrix} \dfrac{\partial \mathbf{r}_s}{\partial u_s} & \dfrac{\partial \mathbf{r}_s}{\partial \theta_s} & -\mathbf{v}_s^{(sw)} \\[2mm] \dfrac{\partial f_{ws}}{\partial u_s} & \dfrac{\partial f_{ws}}{\partial \theta_s} & \dfrac{\partial f_{ws}}{\partial \psi_s}\dfrac{d\psi_s}{dt} \end{bmatrix} \tag{23}$$

has the rank $r = 2$. This results in an equation

$$F_{ws}\left(u_s,\theta_s,\psi_s\right)=0 \tag{24}$$

(4) Equation of meshing (7) and equation (24) permits the sought-for line on Σ_s to be obtained that generates singular points on surface Σ_w.

The computational procedure for the determination and avoidance of worm singularities is as follows:

Step 1:Using equation of meshing (7), we are able to determine the lines of contact of the shaper and the worm in the plane of shaper parameters (u_s, θ_s, ψ_s) as functions of the generalized parameter ψ_s. Fig. 18 illustrates such lines for both sides of shaper space.

Step 2: Using equation (24), we may determine the image of worm singular points in plane (u_s, θ_s, ψ_s) (Fig. 18).

Step 3: Using equations (7) and (24) and equations of the shaper tooth surface, we may determine the lines of shaper regular points that generate the worm singularities.

Step 4: Using coordinate transformation from the shaper surface to the worm thread surface, we may determine: (i) regular points A on the shaper surface (Fig. 19(a)), and (ii) singularity points B on worm surface (Fig. 19(b)) that are generated by points A. Only one line of worm singularity points is represented in Fig. 19(b) due to limitations of rotation angle of the worm.

Singularities of the worm may be avoided by limitation of worm threads as shown in Fig. 19(b).

Dressing of the Worm. The worm dressing is based on generation of its surface Σ_w point by point by a plane or by a conical disk that has the same profile that the rack-cutter that generated the shaper. The execution of motions of the disk or the plane with respect to the worm is accomplished by application of a CNC machine. The determination of instantaneous installments of the grinding disk with respect to the worm requires application of a computer program. The algorithm of the program is based on the following considerations:

(1) The worm thread surface Σ_w is determined as the envelope to the family of shaper surfaces as follows:

$$\mathbf{r}_w = \mathbf{r}_w(u_s, \theta_s, \psi_s), \qquad f_{ws}(u_s, \theta_s, \psi_s) = 0 \tag{25}$$

Equations (25) represent the worm surface by three related parameters

(2) The worm thread surface Σ_w may be represented in two parameter form using the theorem of implicit function system existence as it was discussed above (see vector function (19)). Assume that $\dfrac{\partial f_{ws}}{\partial \theta_s} \neq 0$, at a point $M\left(u_s^{(0)}, \theta_s^{(0)}, \psi_s^{(0)}\right)$. Then equation (7) may be solved in the neighborhood of M by

$$\theta_s = \theta_s(u_s, \psi_s) \in C^1 \tag{26}$$

and the worm surface may be represented as

$$\mathbf{r}_w(u_s, \theta_s(u_s, \psi_s), \psi_s) \tag{27}$$

The computational procedure is as follows:

Step 1: Take $\theta_s = \text{constant}$.
Step 2: Assign u_s and obtain ψ_s from $\theta_s = \theta_s(u_s, \psi_s)$.
Step 3: Compute x_w, y_w, z_w from

$$\mathbf{r}_w(u_s, \theta_s(u_s, \theta_s), \psi_s) \tag{28}$$

Step 4: Knowing u_s, it is easy to get $\mathbf{n}_s(u_s)$ and then determine

$$\mathbf{n}_w(u_s,\theta_s,\psi_s)=\mathbf{L}_{ws}(\theta_s,\psi_s)\mathbf{n}_s(u_s) \tag{29}$$

Step 5: The data ($x_w, y_w, z_w, \mathbf{n}_w$) is sufficient for the installment of the tool (a plane or a disk) using a CNC machine.

Numerical example. The worm design parameters considered for this example are represented in Table 1.

Table 1: Design parameters of grinding worm

Direction of Worm Thread	Right Hand
Number of Worm Thread	$N_w = 1$
Number of teeth of the shaper	$N_s = 30$
Number of teeth of the face gear	$N_2 = 140$
Module	$m = 3.175$ mm
Driving side pressure angle	$\alpha_c = 27.5°$
Coast side pressure angle	$\alpha_c = 27.5°$
Shaft angle	$\gamma_m = 100.0°$
Worm Lead Angle	$\lambda_w = 0.786°$
Shaft Distance between the Shaper and the Worm	$E_{ws} = 68.069$ mm

The numerical values represented in Table 2 are obtained considering $u_s = 0$; $\theta_{min} \leq \theta_s \leq \theta_{max}$ and equations (7) and (24)

Table 2: Numerical values

Point	u_s	θ_s	ψ_s	N_{wx}	N_{wy}	N_{wz}
1		0.701176	-0.232969	-0.359304	0.290277	0.886927
2		0.607726	-0.139518	0.242689	-0.393017	0.886927
3	0	0.514275	-0.046068	-0.098599	0.451263	0.886927
4		0.420824	0.047383	-0.056653	-0.458422	0.886927
5		0.327374	0.140833	0.205491	0.413683	0.886927

Here ψ_s is the angle of rotation of the shaper, N_{wx}, N_{wy} and N_{wz} are the components of the normal to the worm surface in the worm coordinate system S_w at point $M^{(i)}$.

The minimum and the maximum values of θ_s correspond respectively to the bottom and top of the shaper, calculated with the following equations:

$$\theta_i = \sqrt{\left(\frac{r_i}{r_{bs}}\right)^2 - 1} \qquad i = (\max, \min) \tag{30}$$

For the considered numerical example the first singularity point (Fig. 18) occurs when ψ_s reaches the value $\psi_s = 18.3^\circ$. Such a point is located at the bottom of the thread of the worm as shown in Fig. 19(b). This is the maximum value for ψ_s that allows to generate a worm with *regular* points only. The corresponding worm rotation angle is $\psi_w = 549^\circ$ that corresponds to $549/360 = 1.5$ threads of the worm. Considering the two limitations for both sides, we obtain 3.0 as the maximum number of threads.

4. Stress Analysis

Introduction The goals of stress analysis represented in this section are:

(i)   Comparison of bending stresses at the fillet of two versions of face gear design: of the edged and rounded fillets (Fig. 4).

(ii)   Determination of contact and bending stresses and investigation of formation of the bearing contact during the cycle of meshing.

The performed stress analysis is based on finite element method [23] and application of general purpose computer program [5]. Finite element method [23] requires the development of a finite element mesh, definition of slave and master contacting surfaces and establishment of boundary conditions.

The authors' approach for application of finite element analysis has the following advantages:

(a)   The generation of finite element models is performed automatically by using the equations of the tooth surfaces and taking into account the corresponding fillets and portion of the rim. Loss of accuracy due to the development of solid models by using CAD computer programs is avoided.

(b)   The proposed approach does not require an assumption of load distribution in the contact area. The contact algorithm of the general purpose computer program [5] is used to get the contact area and stresses by application of the torque to the pinion. The gear is considered at rest.

(c)   Finite element models are developed numerically at the chosen contact point of the path of contact. Stress convergence is assured because there is at least one point of contact between the contacting surfaces.

(d)   Finite element models of five pairs of teeth are applied and therefore the boundary conditions are far enough from the loaded areas of the teeth.

Development of Finite Element Models. The development of finite element models using CAD computer programs is time expensive, requires skilled users for application of computer programs and has to be done for every case of development of gear geometry and the position of meshing desired for investigation. The approach developed is free of all these disadvantages and is summarized as follows:

Step 1: Using the equations of both sides of tooth surfaces and the portions of the corresponding rim, we may represent analytically the volume of the designed body. Fig. 20(a) shows the designed body for one-tooth model of the pinion of a face-gear drive.

Step 2: Auxiliary intermediate surfaces 1 to 6 as shown in Fig. 20(b) can be determined. Surfaces 1 to 6 divide the tooth in six parts and control the discretization of these tooth subvolumes into finite elements.

Step 3: Analytical determination of node coordinates is performed taking into account the number of desired elements in longitudinal and profile directions (Fig. 20(c)). We emphasize that all nodes of the finite element mesh are determined analytically and the points of intermediate surfaces of the tooth belong to the real gear tooth surfaces.

Step 4: Discretization of the model by finite elements (using the nodes determined in previous step) is accomplished as shown in Fig. 20(d).

Step 5: Setting of boundary conditions for the gear and the pinion are accomplished automatically under the following conditions:

(i)   Nodes on the two sides and bottom part of the portion of the gear rim are considered as fixed (Fig. 21(a))

(ii)   Nodes on the two sides and the bottom part of the pinion rim form a rigid surface (Fig. 21(a) and 21(b)). Such rigid surfaces are three-dimensional structures that may perform translation and rotation but cannot be deformed.

(iii)   The advantage of consideration of pinion rim rigid surfaces mentioned above is as follows: (a) their variables of motion (its translation and rotation) are associated with a single point chosen as the reference point M ; (b) point M is located on the pinion axis of rotation (Fig. 21(b)); (c) reference point M has only one degree-of-freedom (rotation about the pinion axis) and all other degrees-of-freedom are fixed; (d) the torque $\mathbf{T}$ in rotational motion is applied directly to the pinion at its reference node M (Fig. 21(b))

Step 6: The contact algorithm of the finite element analysis computer program [5] requires definition of contacting surfaces. The proposed approach identifies automatically all the elements of the model required for the formation of such surfaces.

The contact algorithm requires as well definition of master and slave surfaces. Generally, the choosing of a master surface is based on the following considerations [5]: (i) it is the surface of the stiffer body of the model, or (ii) the surface with coarser mesh if the contacting surfaces are located on structures with comparable stiffness. We have chosen for stress analysis the gear and pinion tooth surfaces as the master and slave ones, respectively.

Numerical Example. The finite element analysis has been performed for two versions of face gear drives of common design parameters represented in Table 3. The versions correspond to face gear drives with conventional and rounded fillet, respectively (Fig.4)

Table 3: Design parameters of face gear drive

Number of teeth of the pinion	25
Number of teeth of the shaper	28
Number of teeth of the face gear	160
Gear ratio	6.4
Module	6.35 mm
Driving side pressure angle	25.0 deg
Coast side pressure angle	25.0 deg
Shaft angle γ_m	90.0 deg
Inner radius of the face gear	471.0 mm
Outer radius of the face gear	559.0 mm

The finite element mesh of five-pair of teeth of version 2 is represented in Fig. 22. Elements [5] of first order enhanced by incompatible modes to improve their bending behavior have been used to form the finite element mesh.

The total number of elements is 67240 with 84880 nodes. The material is steel with the properties of Young's Modulus $E = 2.068 \times 10^8$ mN/mm^2 and Poisson's ratio 0.29. A torque of 1600 N·m has been applied to the pinion for both versions of face gear drives. Fig. 23 shows the model of the gear drive applied for stress analysis.

Figs. 24 and 25 show the maximum contact and bending stresses obtained at the mean contact point for gear drives of two versions of fillet (see Fig. 4). It is confirmed that the bending stresses are reduced more than 10% for the face-gear with a rounded fillet in comparison to the fillet generated by the edge of the shaper.

The stress analysis performed has been complemented with investigation of formation of the bearing contact (Figs. 25 and 26). The results obtained show the possibility of an edge contact in face gear drives by application of involute pinion. Avoidance of edge contact requires the changing of the shape of the pinion profiles.

Fig. 26 illustrates the variation of bending and contact stresses of the gear and the pinion during the cycle of meshing. The stresses are represented as functions of unitless parameter ϕ represented as

$$\phi = \frac{\phi_P - \phi_{in}}{\phi_{fin} - \phi_{in}}, \qquad 0 \le \phi \le 1 \tag{31}$$

Here: ϕ_P is the pinion rotation angle, ϕ_{in} and ϕ_{fin} are the magnitudes of the pinion angular positions in the beginning and end of cycle of meshing.

The unitless stress coefficient σ (Fig. 26}) is defined as

$$\sigma = \frac{\sigma_P}{\sigma_{P_{max}}}, \qquad |\sigma| \le 1 \tag{32}$$

Here: ϕ_P is the variable of function of stresses and $\phi_{P_{max}}$ is the magnitude of maximal stress. The increase of contact stresses during the cycle of meshing is caused by the edge contact.

5. Conclusions

Based on the research performed , the following conclusions may be drawn:

(1) An analytical approach for determination of the worm thread surface, avoidance of singularities and worm dressing have been proposed.

(2) Computer programs for generation of face gears by application of grinding or cutting worms have been developed. These computer programs cover also tooth contact analysis and stress analysis of face gear drives.

(3) Automatization of the development of finite element models is proposed and the most time-consuming step in application of finite element analysis, the design of contacting models by using CAD computer programs, is avoided.

(4) Generation of face gears by a shaper or grinding worm with rounded top edge is proposed to reduce bending stresses. Computations confirm that the bending stress can be reduced approximately 10%.

References

[1] Argyris, J., Litvin, F. L., Lian, Q., and Lagutin, S. A., *Determination of Envelope to Family of Planar Parametric Curves and Envelope Singularities,* Journal Computer Methods in Applied Mechanics and Engineering, Vol. 175, No. 1-2, pp. 175-187, 1999.

[2] Argyris, J., Litvin, F.L., Peng, A., and Stadtfeld, H.J., *Axes of Meshing and Their Application in Theory of Gearing,* Journal Computer Methods in Applied Mechanics and Engineering, Vol. 163, No. 1-4, pp. 293-310, 1998.

[3] Baumann, V., Bär, G., Haase, A., Hutschenreiter, B., Hünecke, C., and Dutschk, R., *BECAL 2.0 Programm zur Berechnung der Zahnflankenund Zahnfu β beanspruchung an Kegelrad- und Hypoidgetrieben bei Berücksichtigung der Verformungen und Abweichungen der Getriebe-elemente},* FVA-Heft 548, Forschungsvereinigung Antriebstechnik, 1998.

[4] Bär, G., *Curvatures of the Enveloped Helicoid,* Mechanism and Machine Theory, Vol. 32, No. 1, pp. 111-120, 1997.

[5] Hibbit, Karlsson & Sirensen, Inc., *ABAQUS/Standard 6.1 User's Manual,* 1800 Main Street, Pantucket, RI 20860-4847, 1998.

[6] Korn, G. A. and Korn, T. M., *Mathematics Handbook for Scientist and Engineers*, McGraw-Hill, Inc., 2nd Ed., 1968.

[7] Litvin, F. L., *Theory of Gearing,* NASA RP-1212 (AVSCOM 88-C-C035), Washington, D. C., 1989.

[8] Litvin, F. L., *Gear Geometry and Applied Theory,* Prentice Hall, Inc., Englewood Cliffs, New Jersey, 1994.

[9] Litvin, F. L., *Development of Gear Technology and Theory of Gearing,* NASA Reference Publication 1406, ARL-TR-1500, 1998.

[10] Litvin, F. L., Demenego, A., and Vecchiato, D., *Formation by Branches of Envelope to Parametric Families of Surfaces and Curves,* Journal Computer Methods in Mechanics and Engineering, Vol. 190, pp. 4587-4608, 2001.

[11] Litvin, F. L., Egelja, A. M., and De Donno, M., *Computerized Determination of Singularities and Envelopes to Family of Contact Lines on Gear Tooth Surface,* Journal Computer Methods in Applied Mechanics and Engineering, Vol. 158, No. 1-2, pp.~23-34, 1998.

[12] Litvin, F. L., De Donno, M., Peng, A., Vorontsov, A., and Handschuh, R. F., *Integrated Computer Program for Simulation of Meshing and Contact of Gear Drives,* Computer Methods in Applied Mechanics and Engineering, Vol. 181, No. 1-3, pp. 71-85, 2000.

[13] Litvin, F. L., Peng, A., and Wang, A. G., *Limitation of Gear Tooth Surfaces by Envelopes to Contact Lines and Edge of Regression,* Mechanism and Machine Theory, Vol. 34, No. 6, pp. 889-902, 1999.

[14] Litvin, F. L., Chen,Y.-J., Heath, G. F., Sheth, V. J., Chen, N., *Apparatus and Method for Precision Grinding Face Gears,* USA Patent 6,146,253, 2000.

[15] Miller, E. W., *Hob for Generation Crown Gears,* USA Patent 2,304,588, 1942.

[16] Sheveleva, G. I., *Mathematical simulation of spiral bevel gear production and meshing processes with contact and bending stresses,* In Proc. IX World Congr. IFToMM, Vol. 1, pp. 509-513, 1995.

[17] Stadtfeld, H. J., *Handbook of Bevel and Hypoid Gears: Calculation, Manufacturing, and Optimization,* Rochester Institute of Technology, Rochester, New York, 1993.

[18] Stosic, N., *On Gearing of Helical Screw Compressor Rotors*, Proc IMechE, Journal of Mechanical Engineering Science, Vol. 212, pp. 587-594, 1998.

[19] Stosic, N., *Recent developments in screw compressors*, Proc IMechE, Journal of Mechanical Engineering Science, C542/066, 1999.

[20] Stosic, N. and Hanjalic, K., *Development and Optimization of Screw Machines With a Simulation Model. Part I: Profile generation*, ASME Transactions, Journal of Fluids Engineering, Vol. 119, pp. 659-663, 1997.

[21] Zalgaller, V. A., *Theory of Envelopes*, Publishing House Nauka (in Russian), 1975.

[22] Zalgaller, V. A. and Litvin, F. L., *Sufficient Condition of Existence of Envelope to Contact Lines and Edge of Regression on the Surface of the Envelope to the Parametric Family of Surfaces represented in Parametric Form*, Proceedings of Universities: Mathematics (in Russian), Vol. 178, No. 3, pp. 20-23, 1977.

[23] Zienkiewicz, O. C. and Taylor, R. L., *The Finite Element Method*, John Wiley & Sons, 5th Ed., 2000.
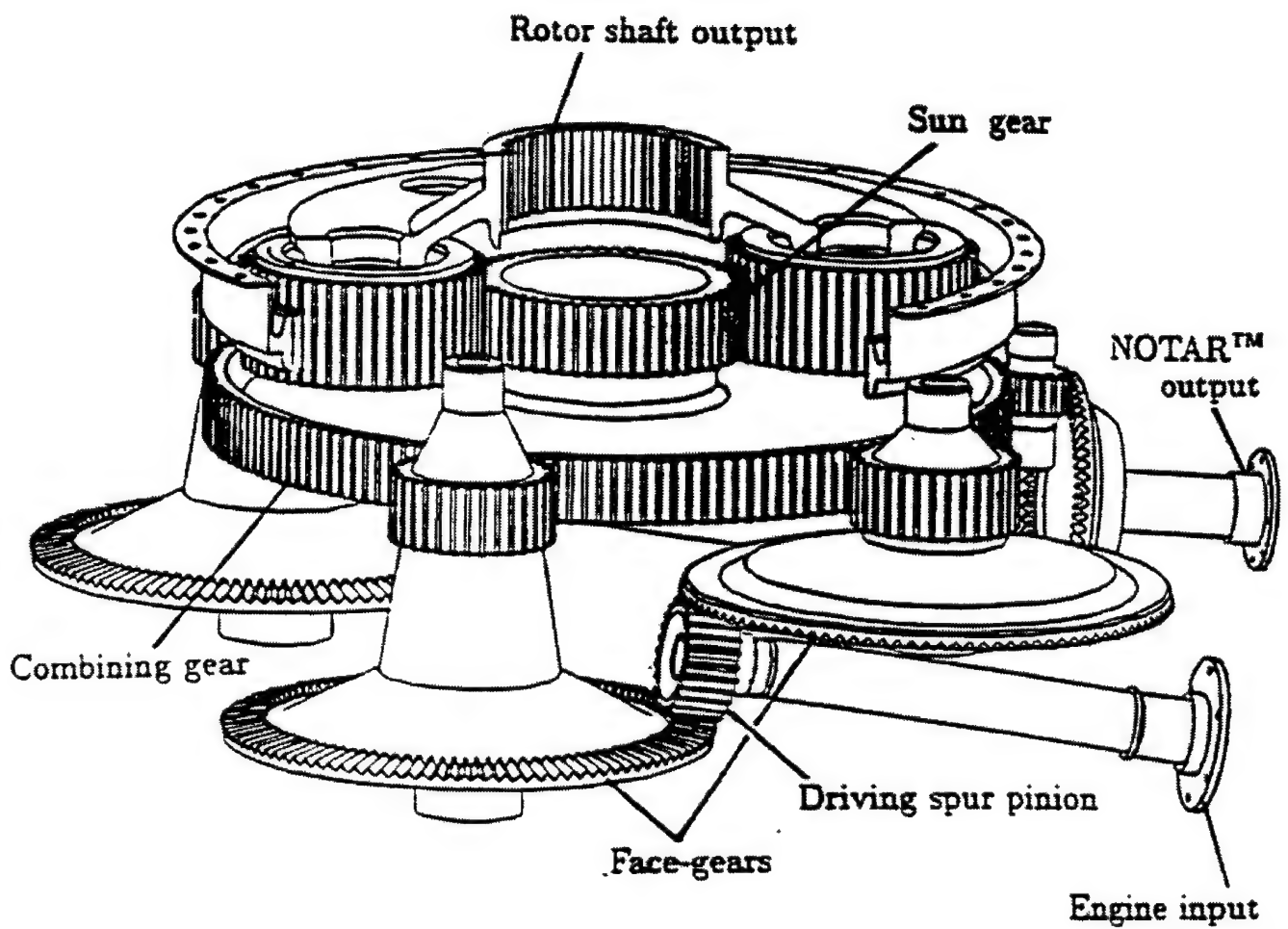
Figure 1: Application of face gear drive in helicopter transmission
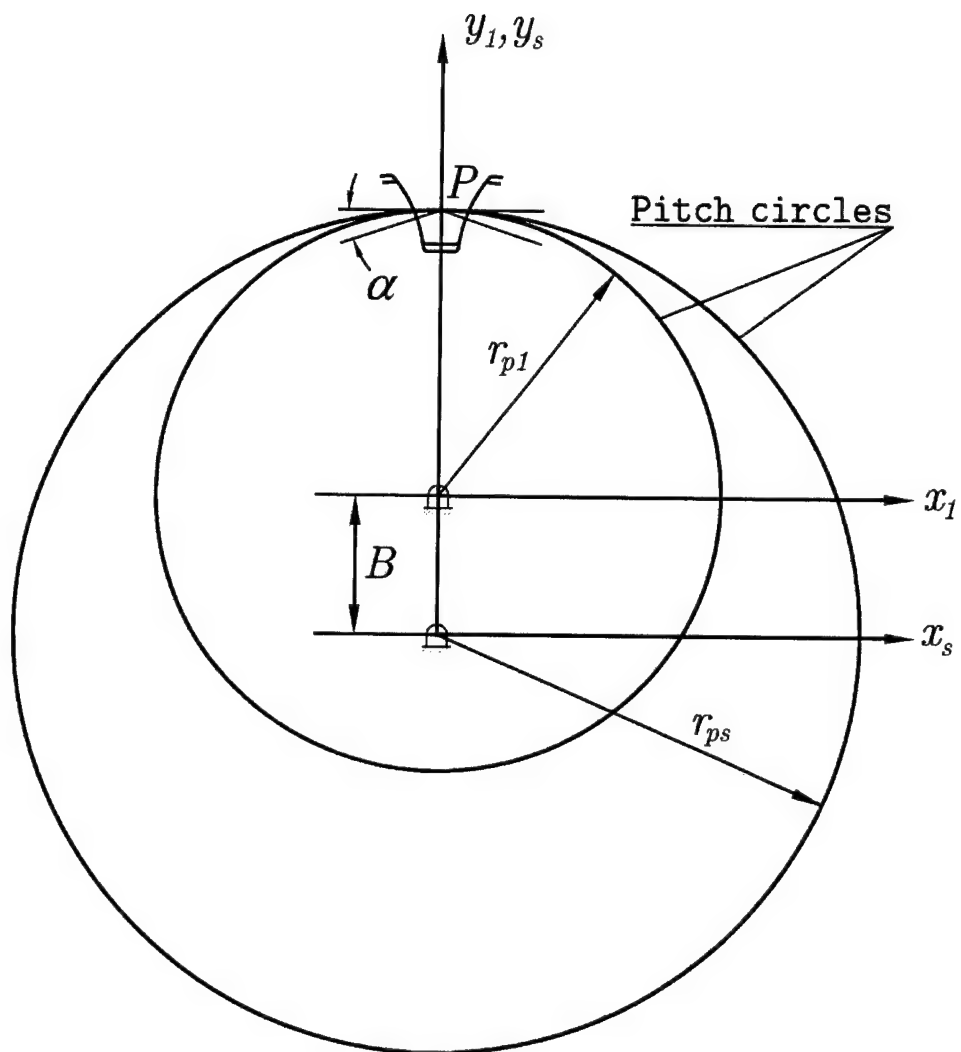
Figure 2: Pitch circles and tooth profiles of pinion and shaper

Fillet
Surface

Contact lines L_{2s}

L^*
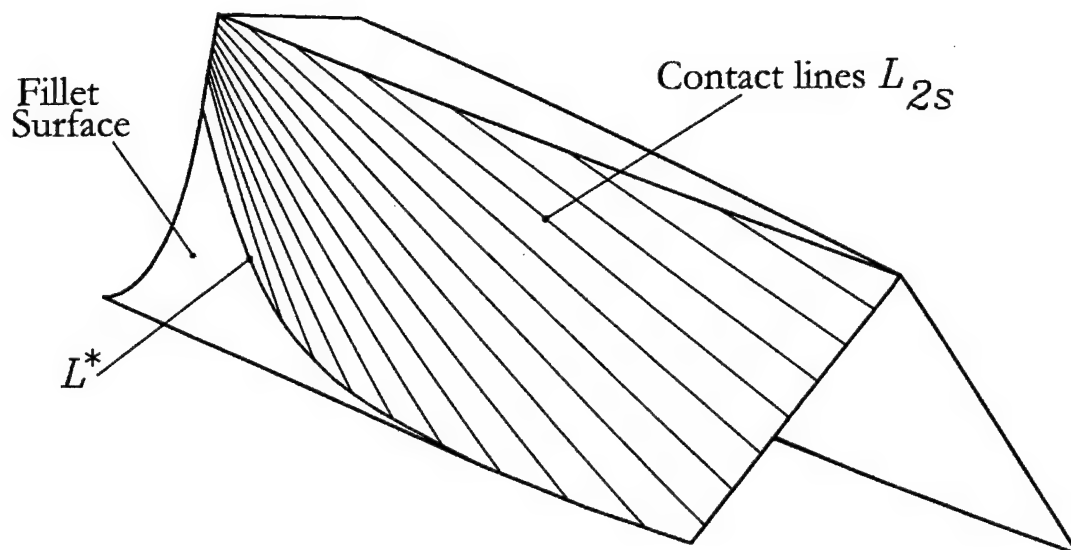
(a)
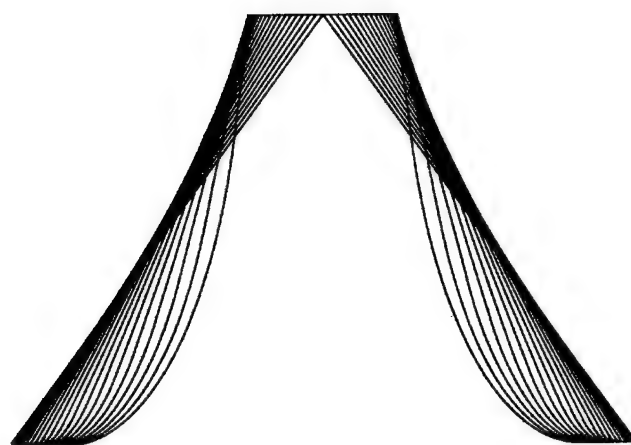
(b)

Figure 3: Structure of face-gear tooth: (a) lines contact L_{2s} and fillet; (b) cross-section of face-gear tooth
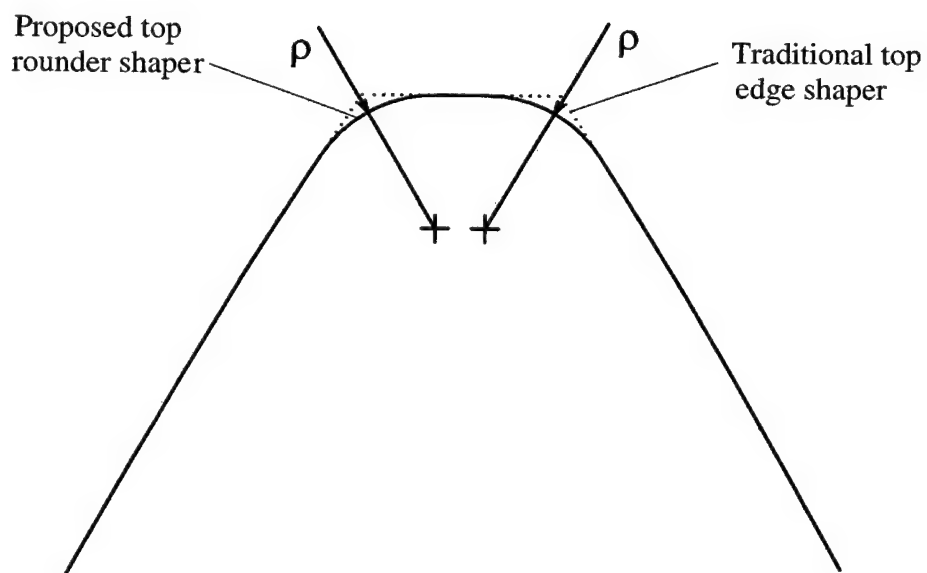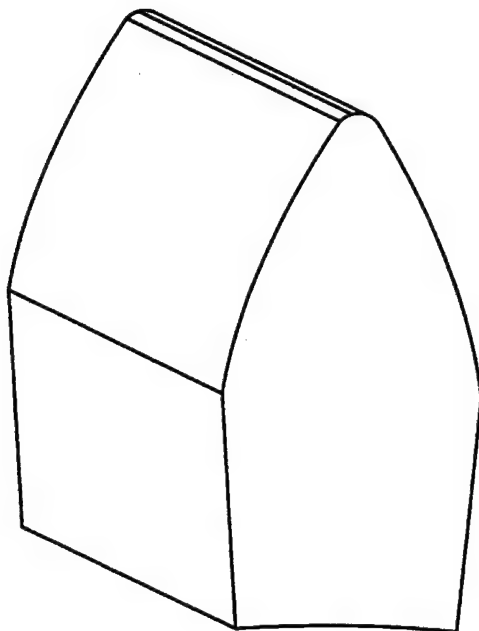
Figure 4: Shaper with a rounded edge
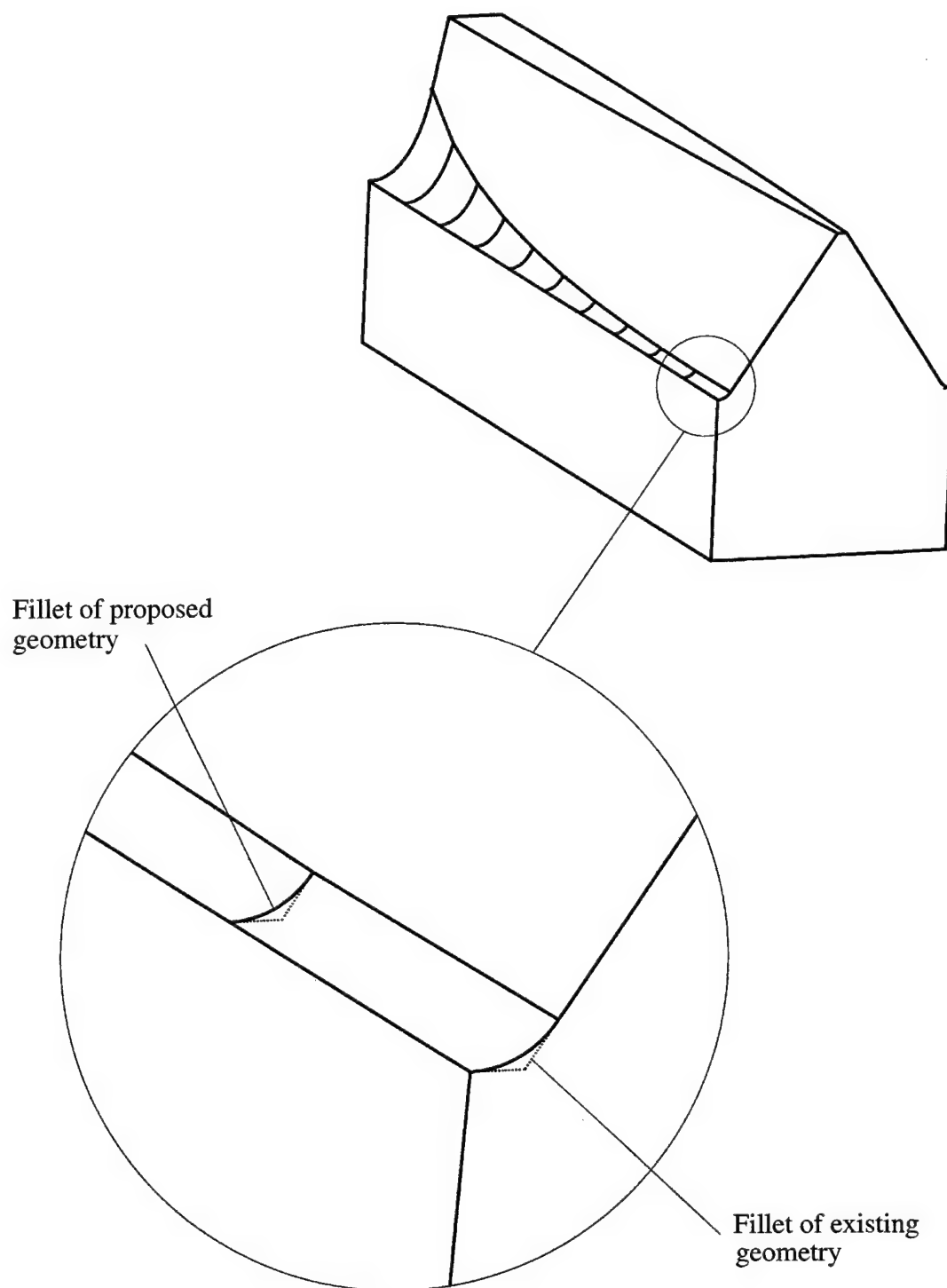
Figure 5: Shape of the modified fillet of the face-gear
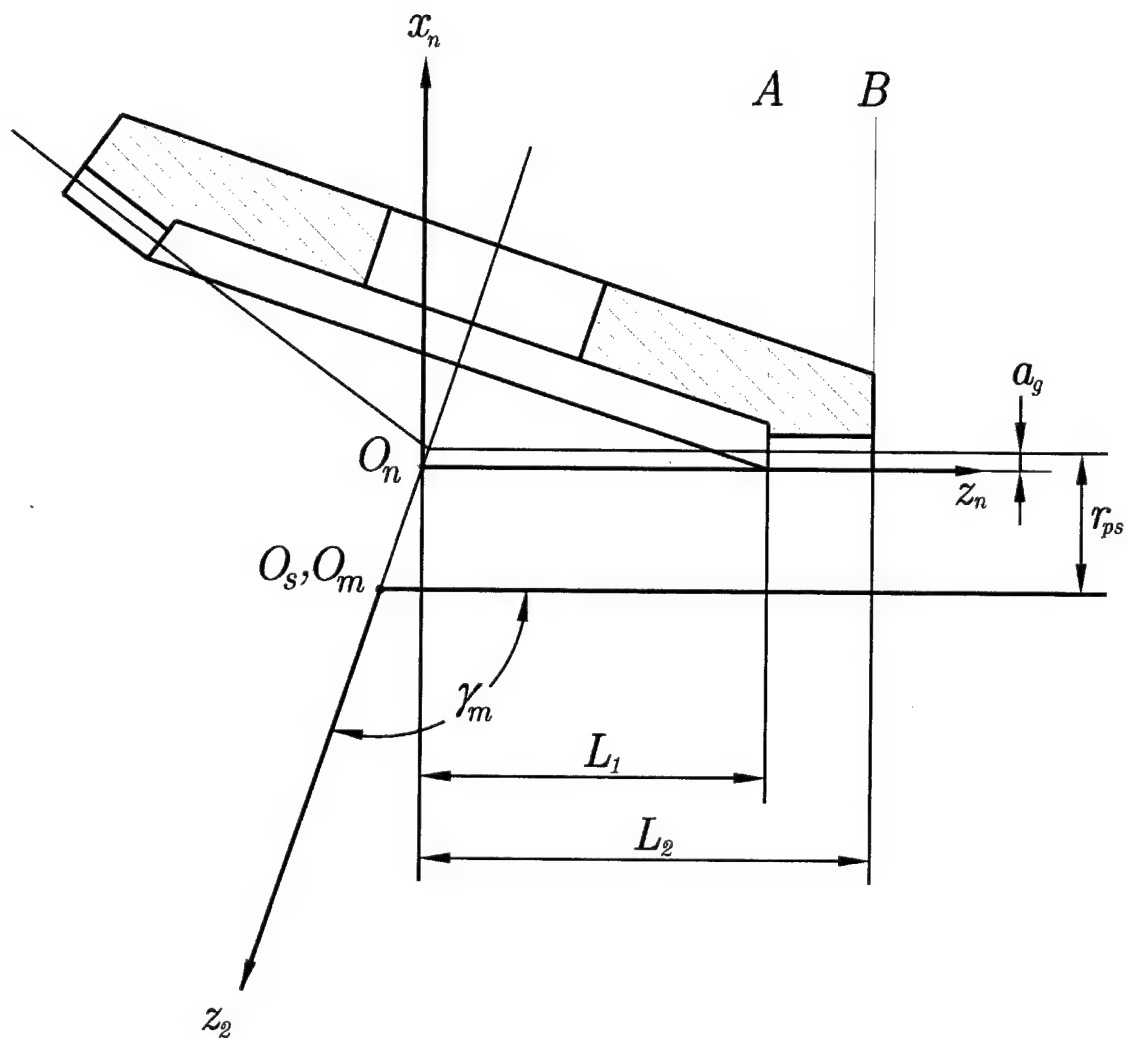
Figure 6: Limitation of length of tooth of face-gear
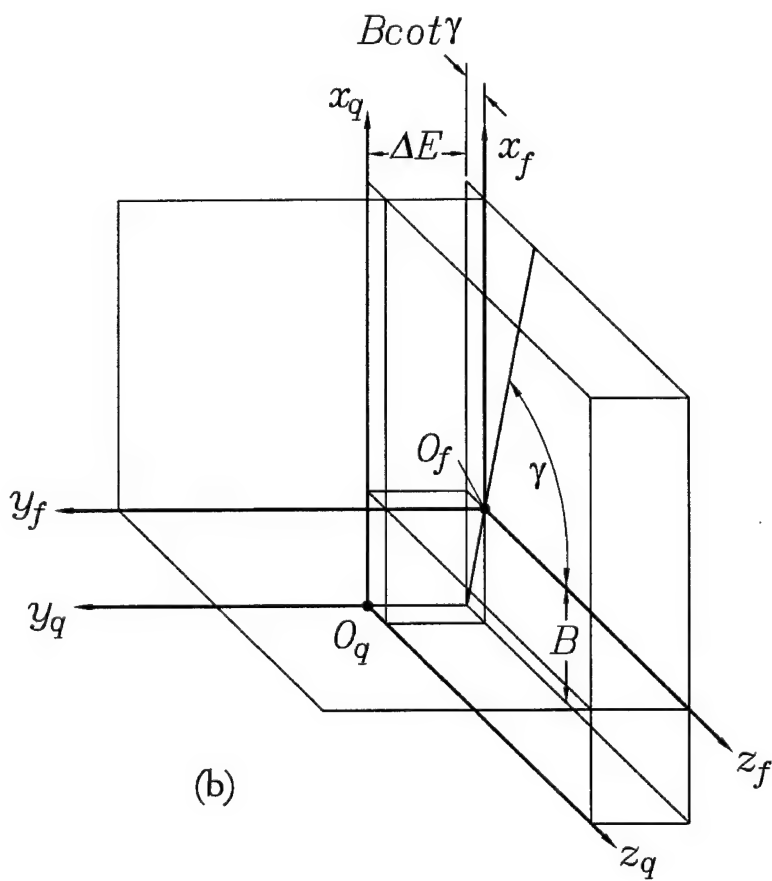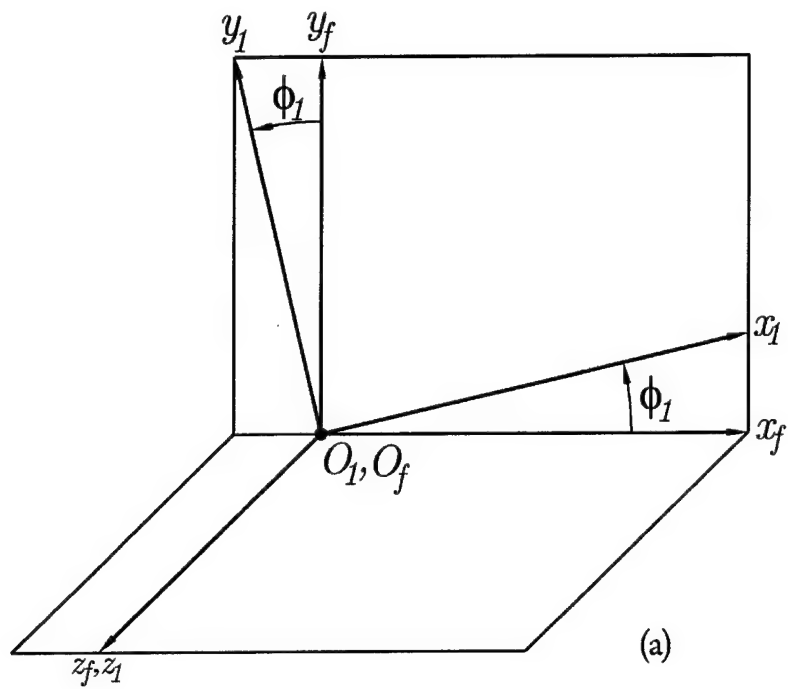
Figure 7: Coordinate systems applied for simulation of meshing: (a) coordinate systems S_1 and S_f; (b) coordinate systems S_f and S_q
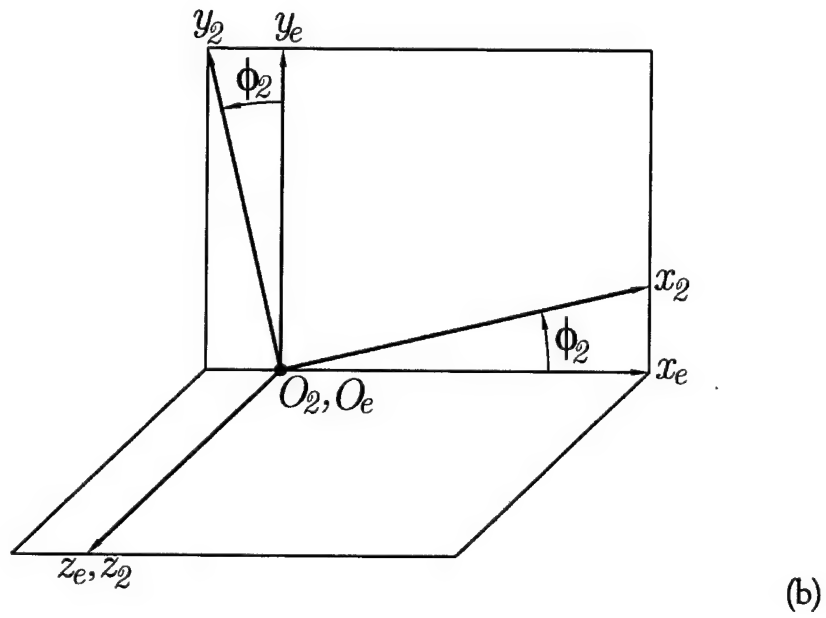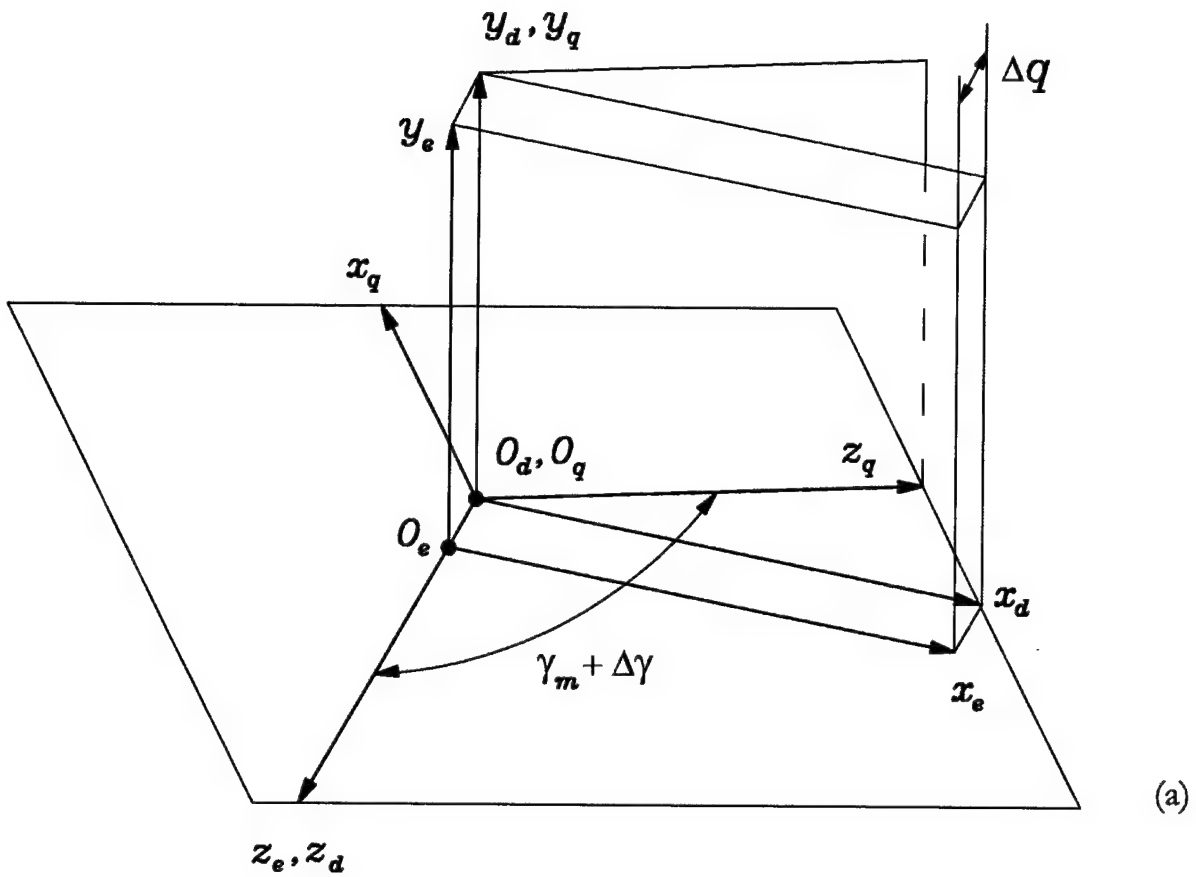
Figure 8: Coordinate systems applied for simulation of meshing: (a) coordinate systems S_q, S_d, S_e; (b) coordinate systems S_2, S_e
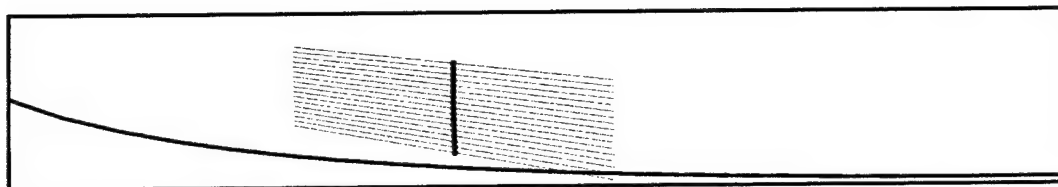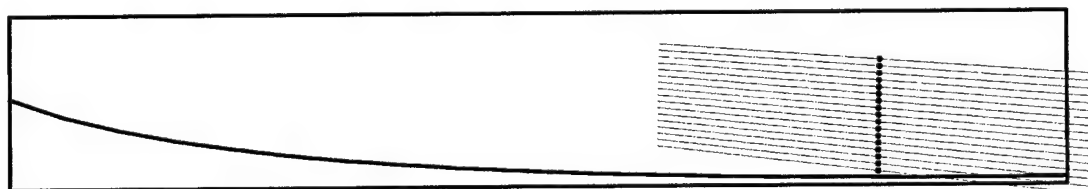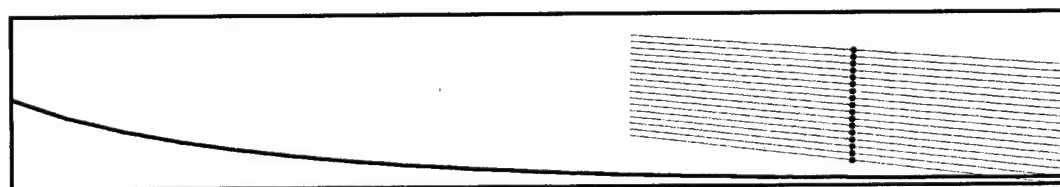
Figure 9: Path of contact and bearing contact for the following examples: (a) No errors of alignment; (b) $|\Delta\gamma| = 3\,\text{arcmin}$; (c) $|\Delta E| = 1000\,\mu m$
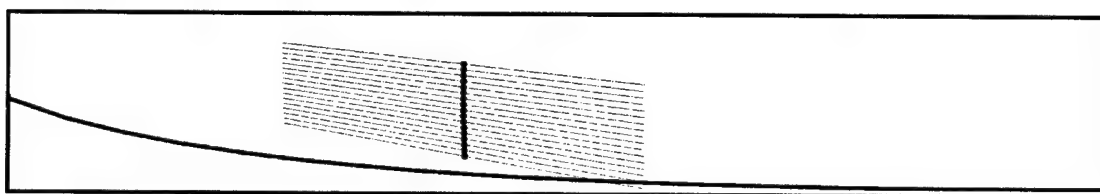
(a)
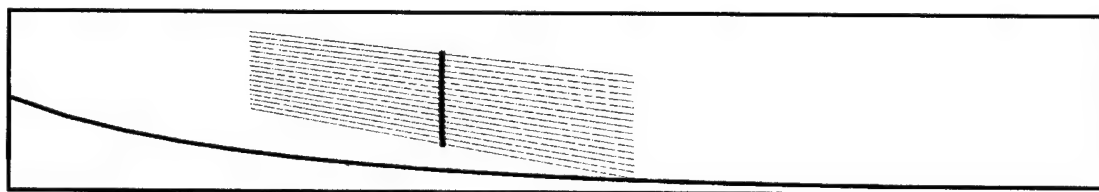
(b)
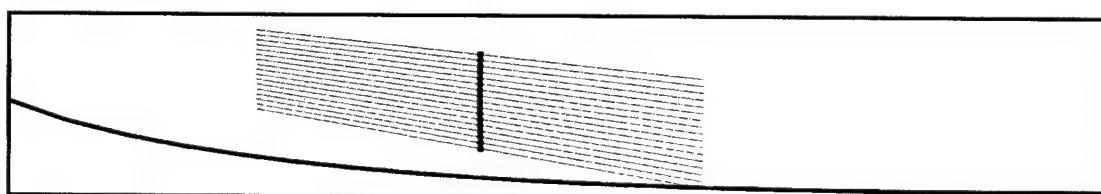
(c)

Figure 10: Adjustment of path of contact by applying the axial displacement Δq of the face gear with respect to the pinion: (a) $|\Delta \gamma| = 3 \, \text{arcmin}$, $|\Delta q| = 550 \, \mu m$; (b) $|\Delta E| = 1000 \, \mu m$, $|\Delta q| = 500 \, \mu m$; (c) $|\Delta \gamma| = 3 \, \text{arcmin}$, $|\Delta E| = 1000 \, \mu m$, $|\Delta q| = 1000 \, \mu m$
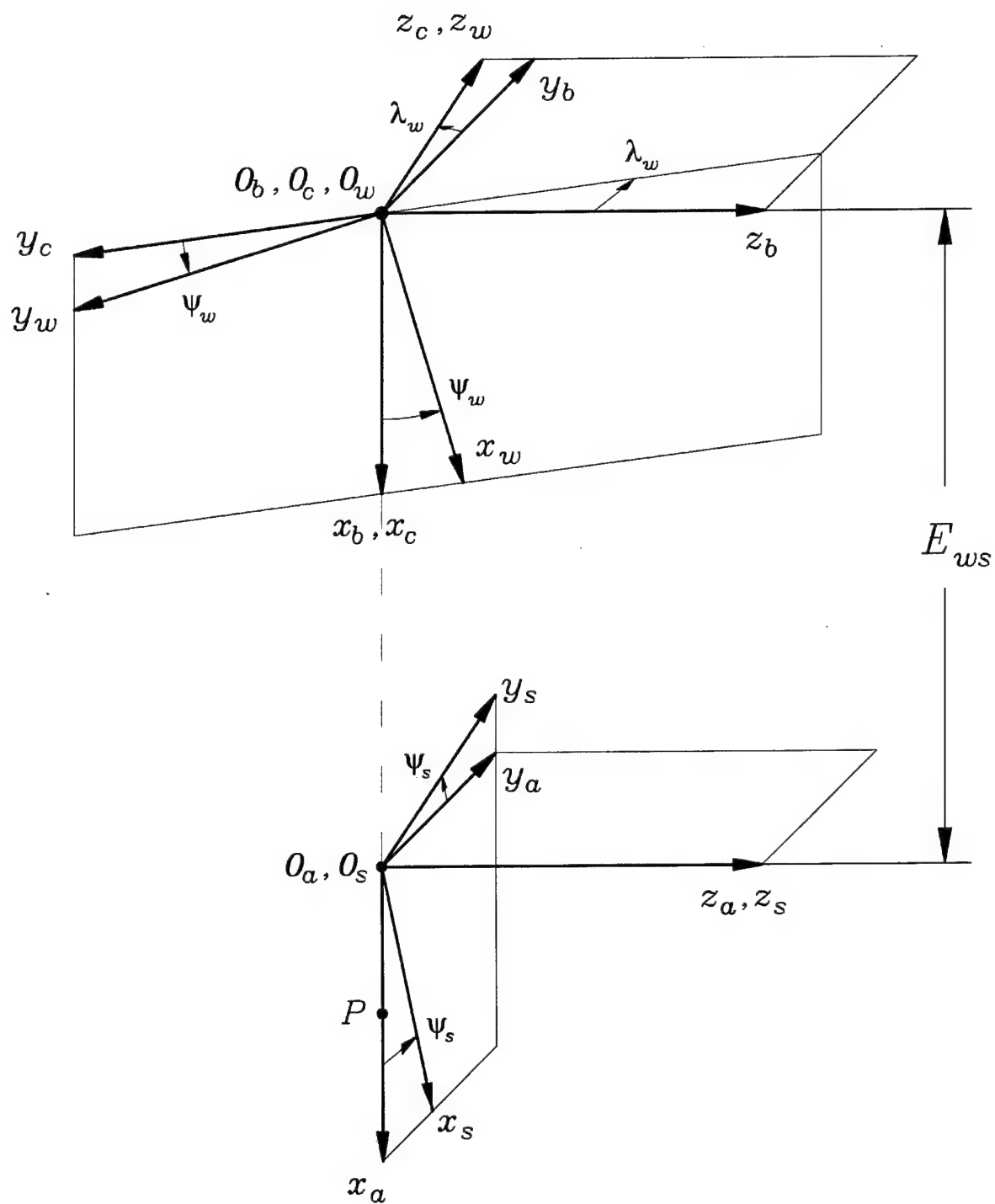
Figure 11: Coordinate systems S_s and S_w and worm installment
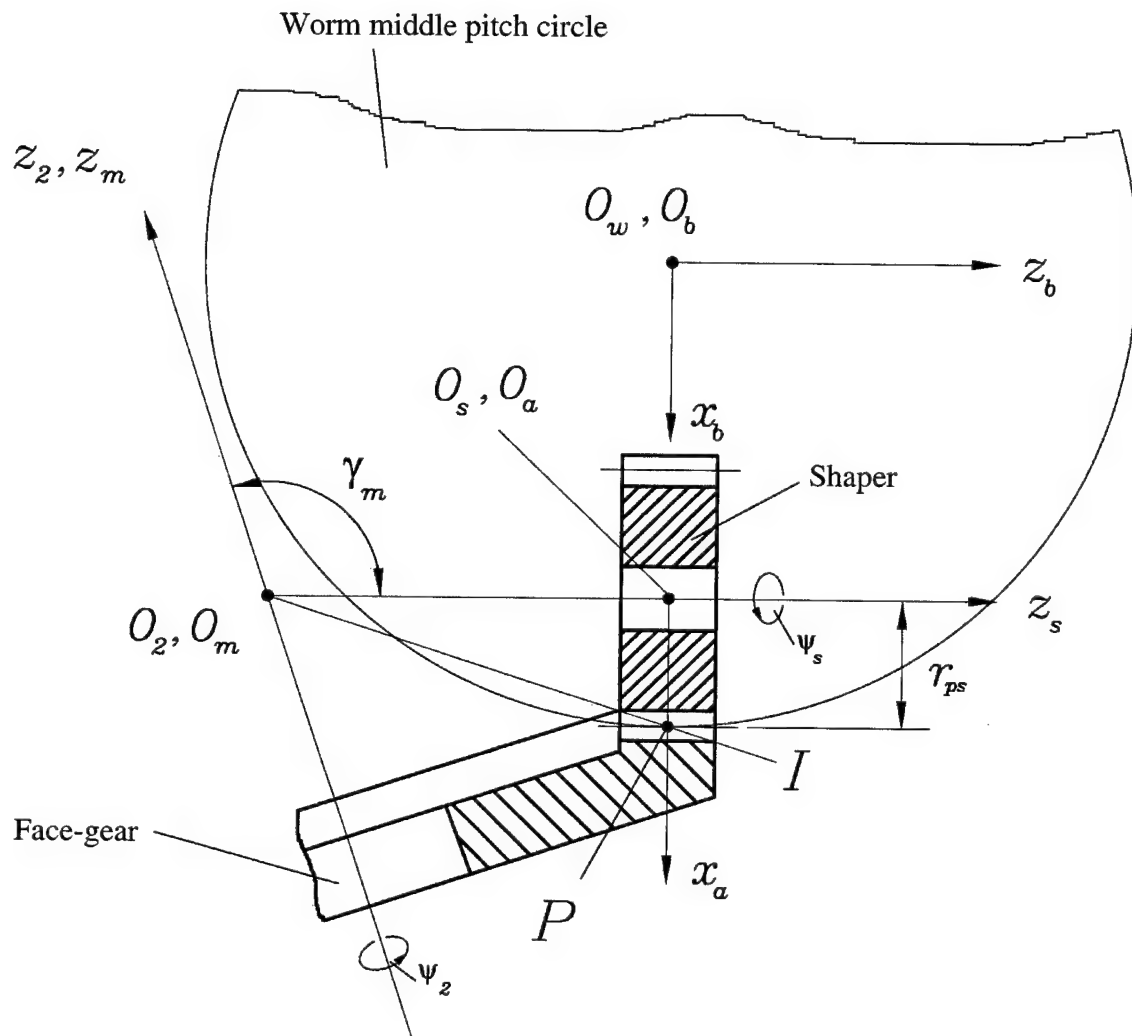
Figure 12: For derivation of tangency of surfaces Σ_s and Σ_2 and generation of the face-gear by the worm
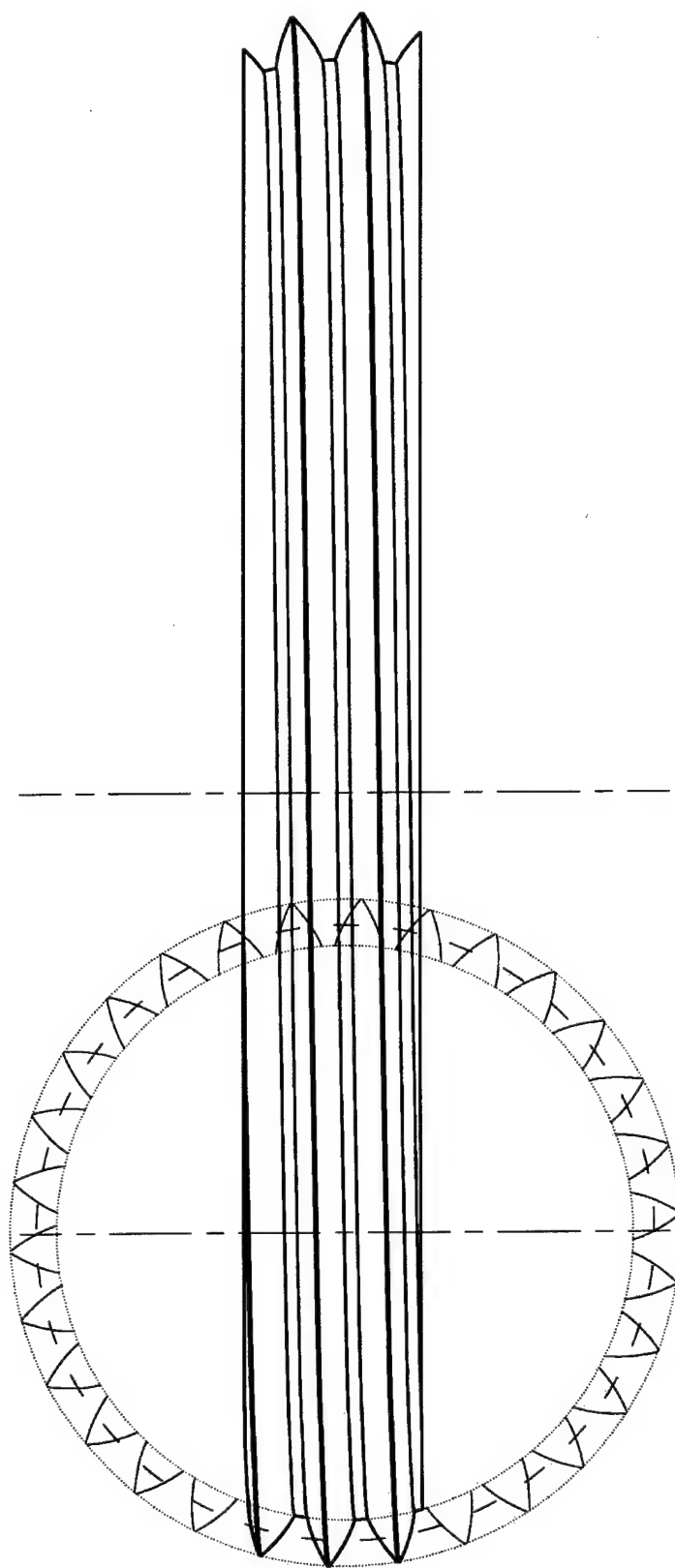
Figure 13: Schematic illustration of meshing of the shaper and the worm
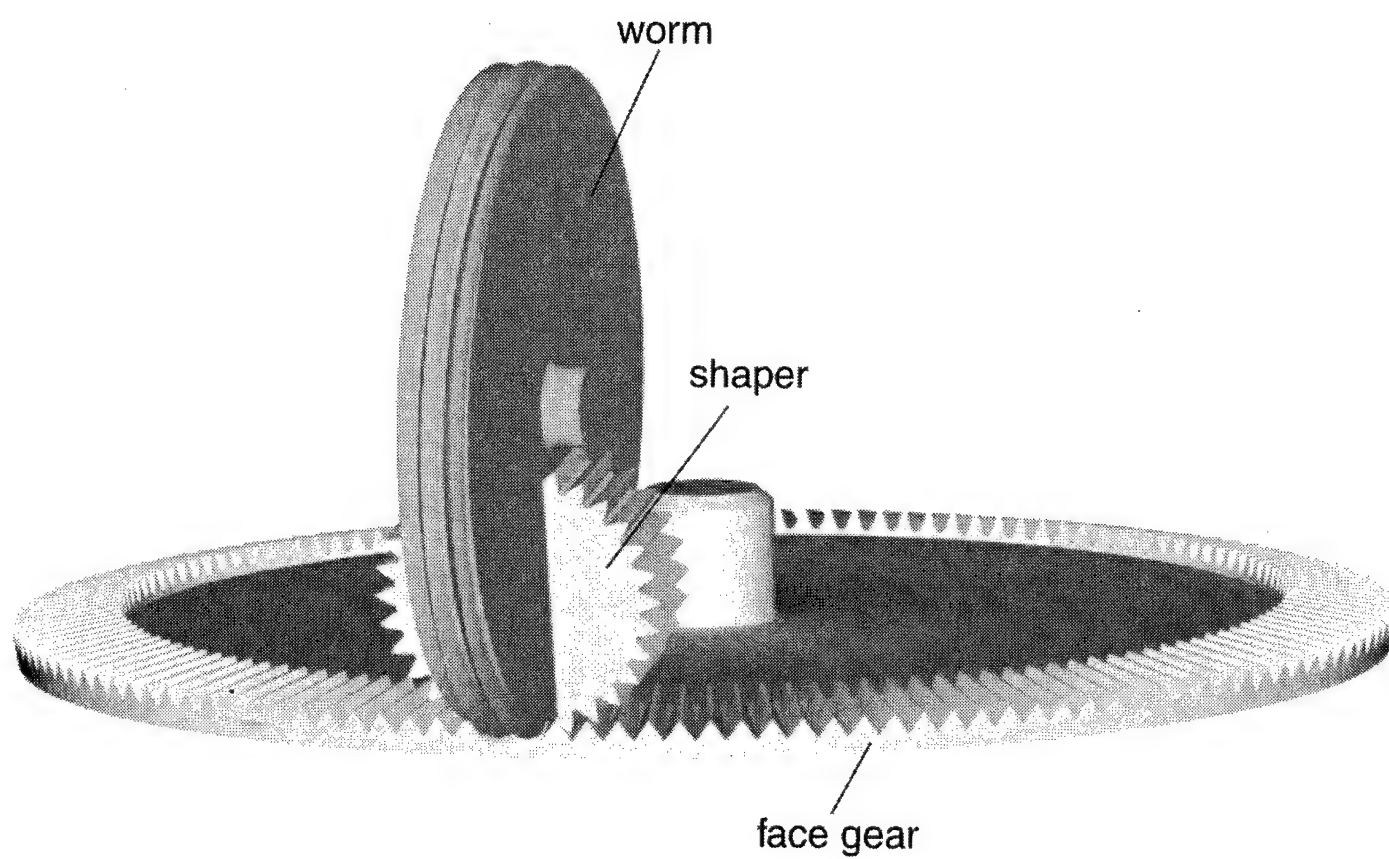
Figure 14: Illustration of simultaneous meshing of shaper, worm, and face-gear
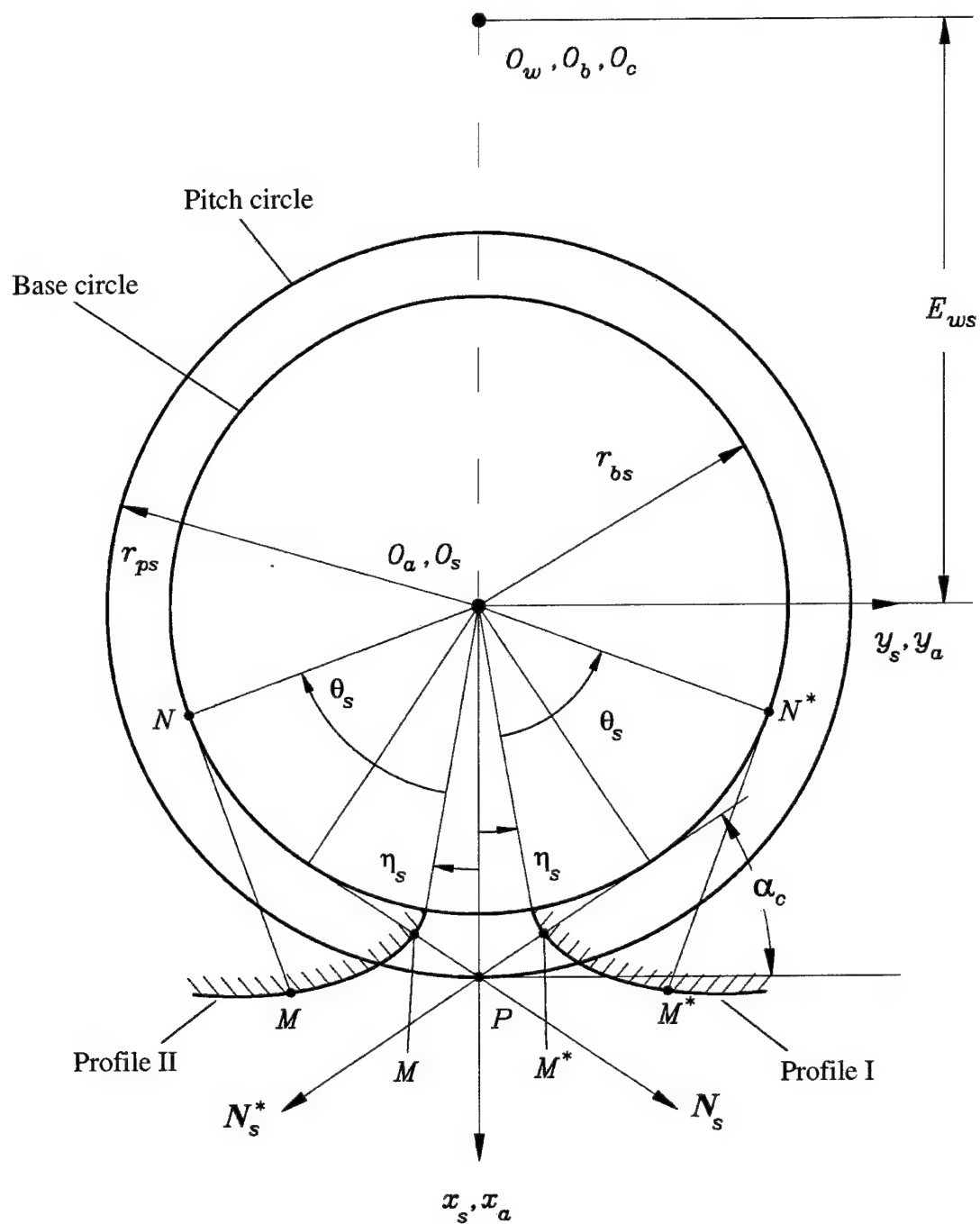
Figure 15: Shaper profiles and normals to shaper profiles
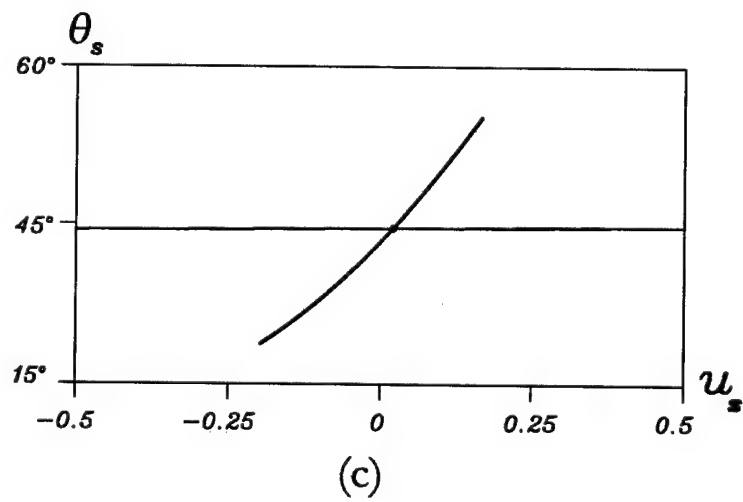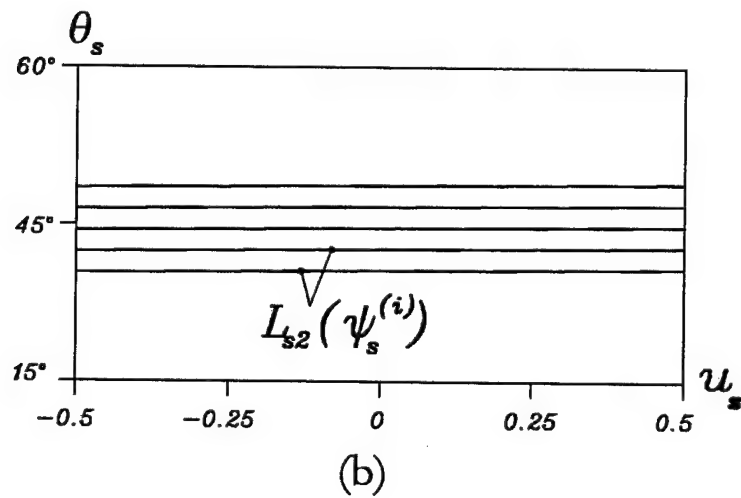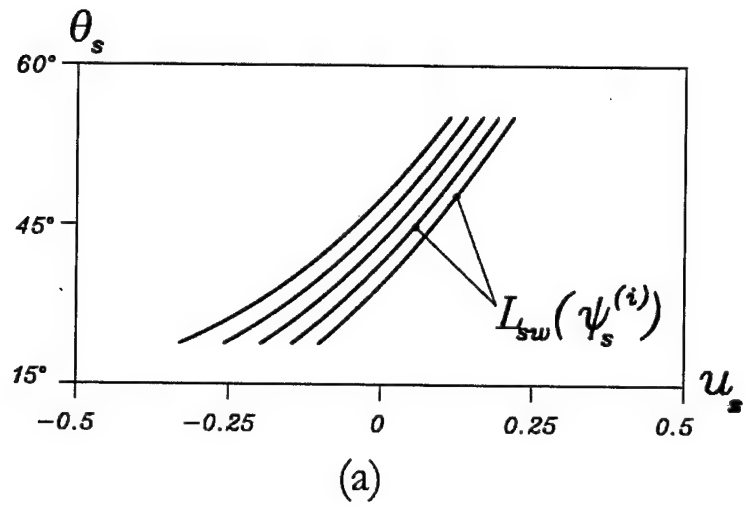
Figure 16: Illustration of lines of tangency (a) lines L_{sw} of tangency of Σ_s and Σ_w; (b) lines L_{s2} of tangency of Σ_s and Σ_2, (c) intersection of L_{sw} and L_{s2}
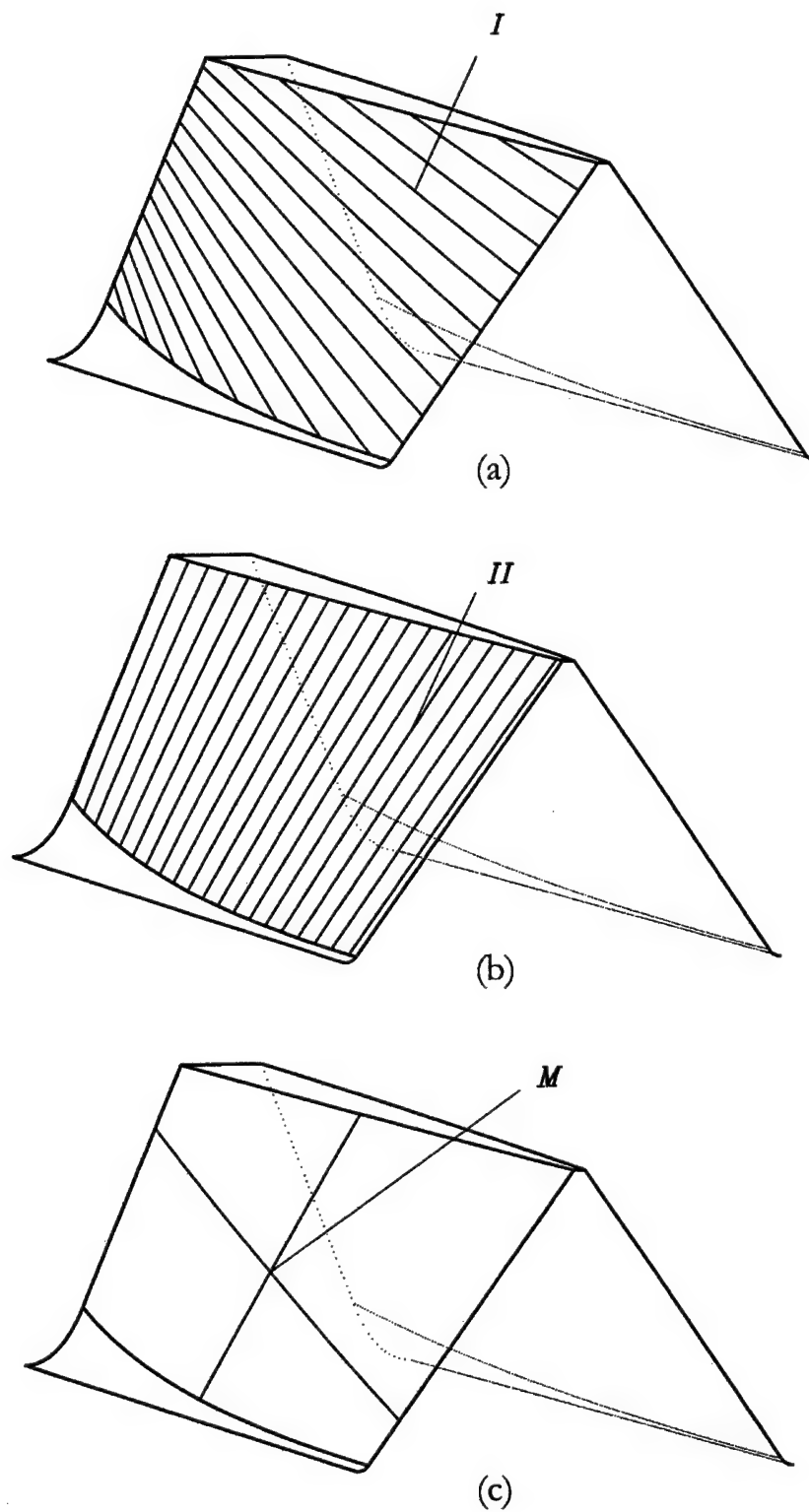
Figure 17: For illustration of meshing of surfaces Σ_2 and Σ_w: (a) lines of tangency of Σ_2 and Σ_w wherein $\psi_w = \text{constant}$, (b) lines of tangency of Σ_2 and Σ_w wherein $l_w = \text{constant}$ and (c) point M of tangency of Σ_2 and Σ_w
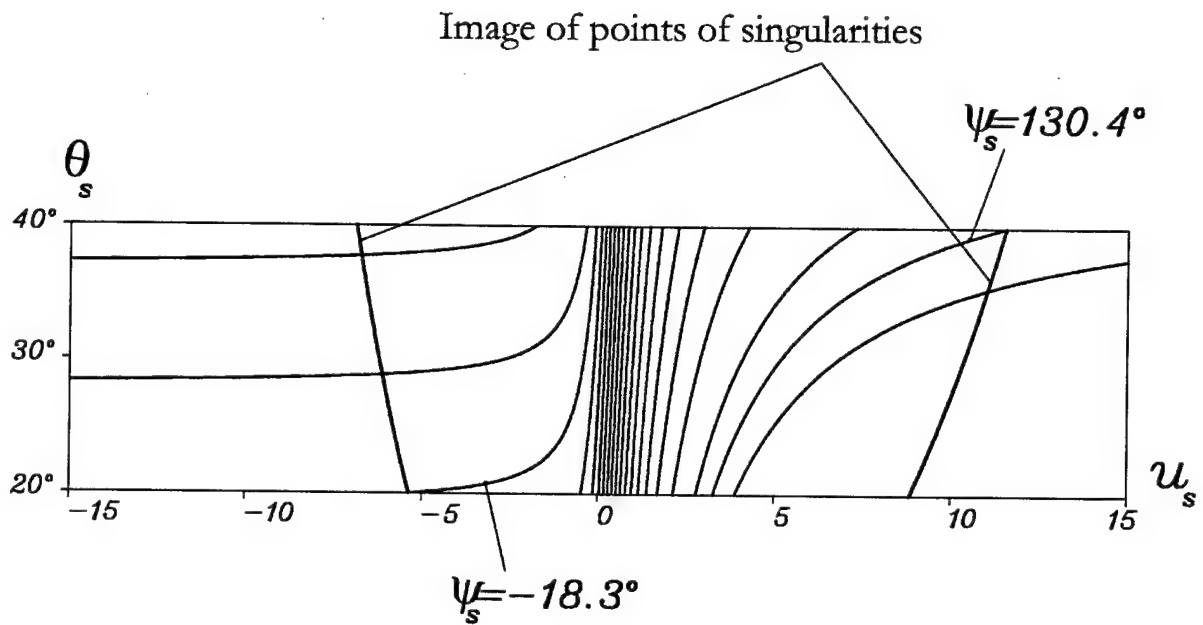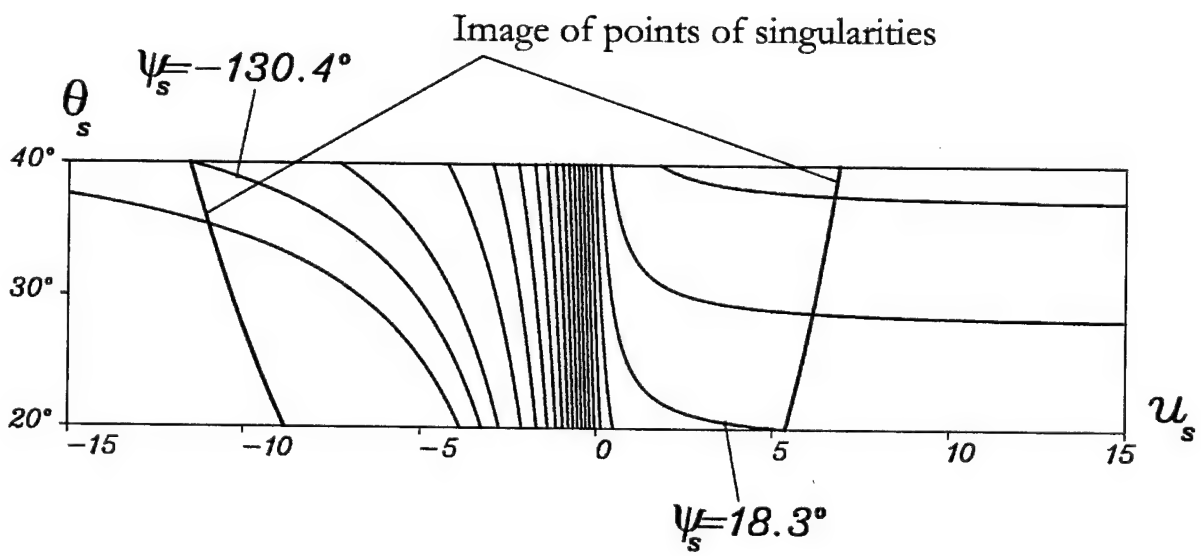
Figure 18: Contact lines between the shaper and the worm in plane (u_s, θ_s): (a) for surface shaper with profile I, and (b) profile II (see Fig. 14)
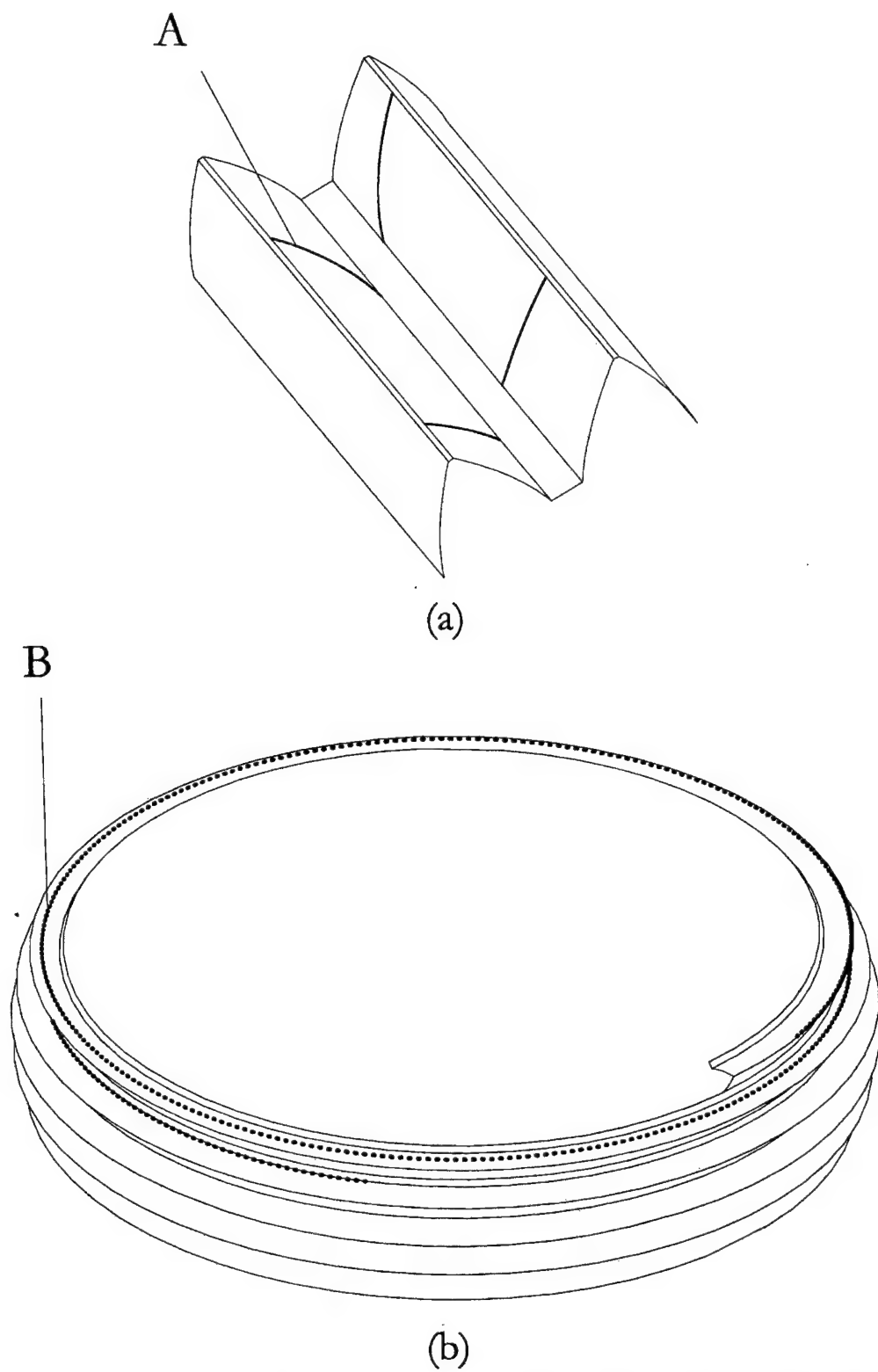
Figure 19: Illustration of worm singularities: (a) regular points A of shaper that generate worm singularities; (b) singularities B on worm threads surface
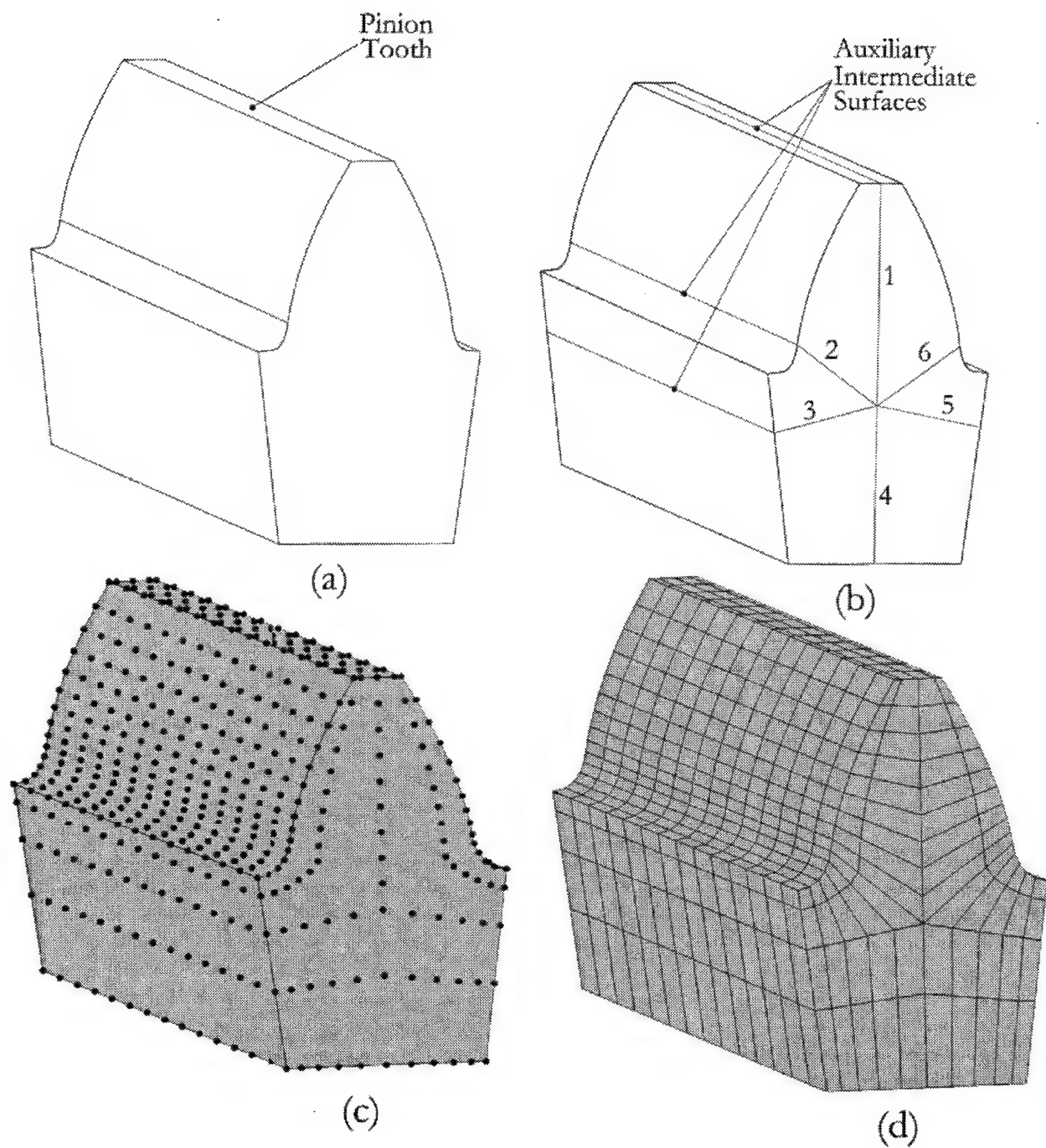
Figure 20: Illustrations of: (a) the volume of designed body, (b) auxiliary intermediate surfaces, (c) determination of nodes for the whole volume, and (d) discretization of the volume by finite elements
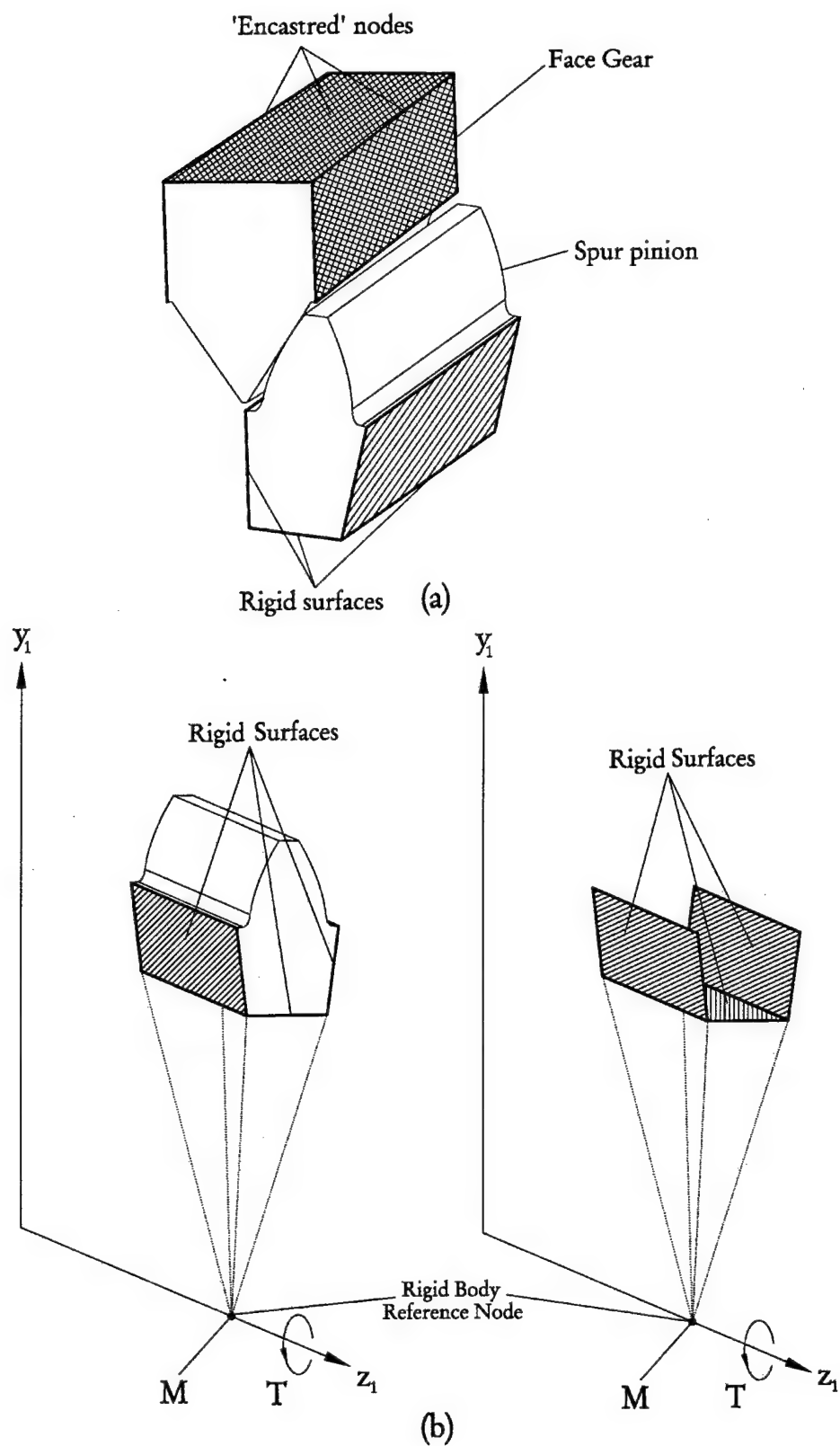
Figure 21: Schematic illustration of: (a) boundary conditions for the pinion and the face-gear, and (b) rigid surfaces applied for boundary conditions of the pinion
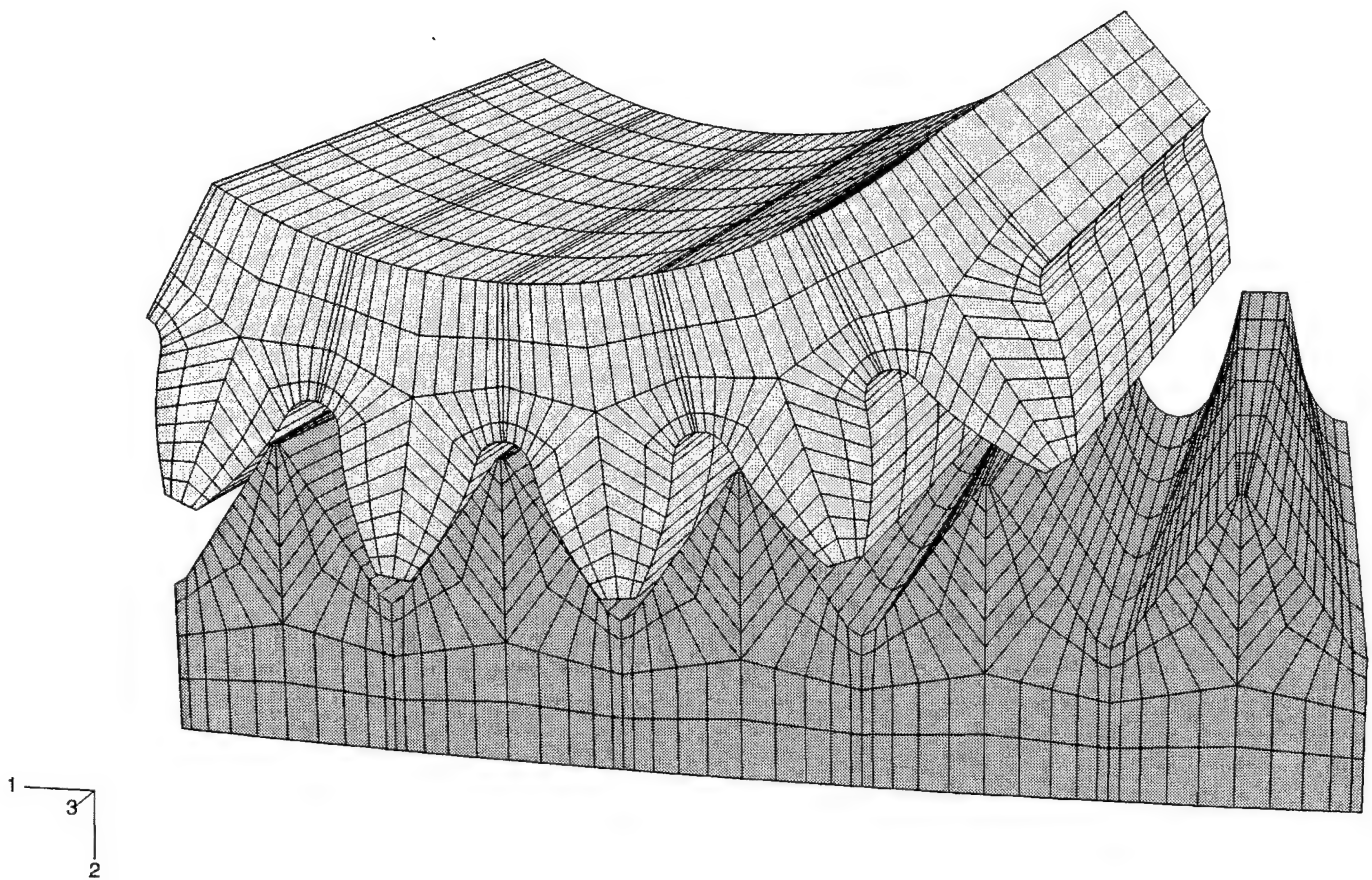
Figure 22: Five-pairs-of-teeth face-gear drive model
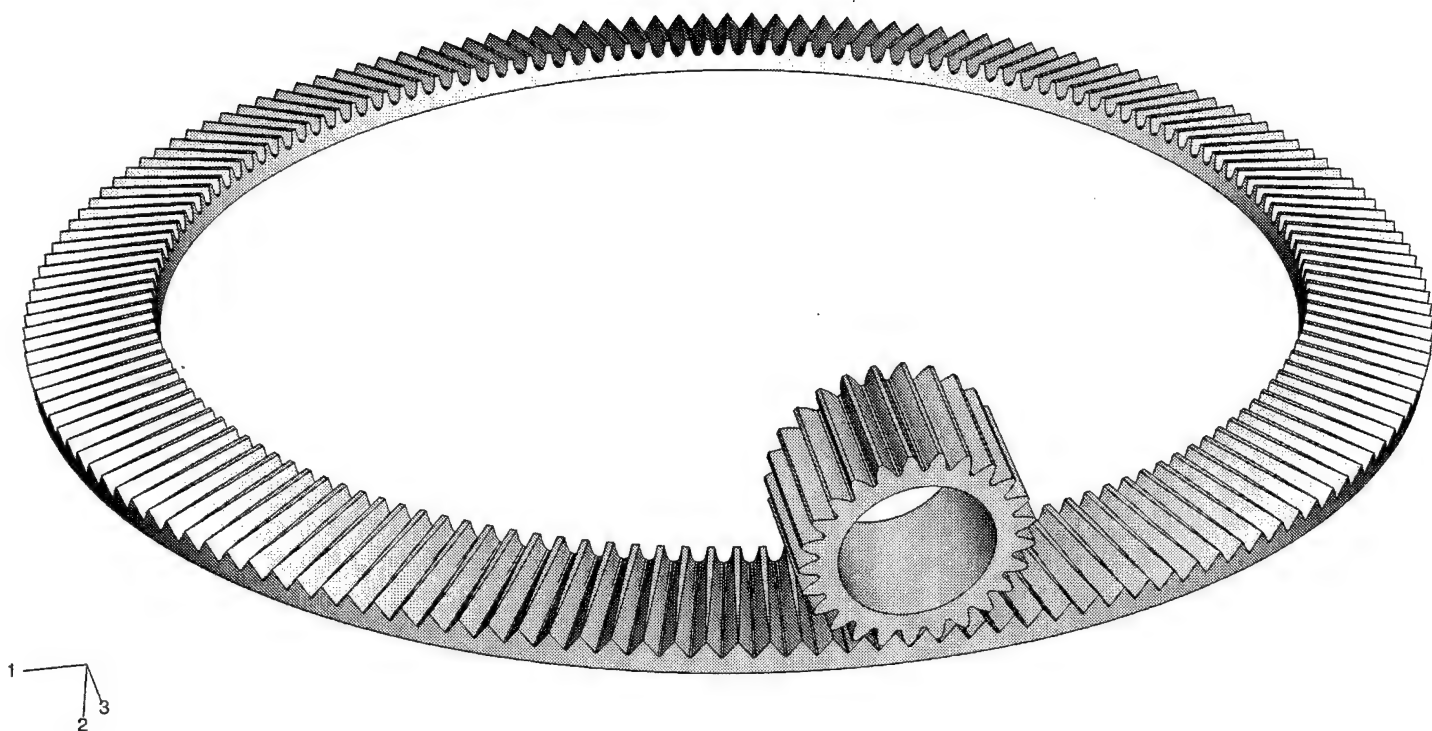
Figure 23: Whole gear drive model
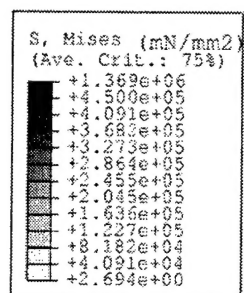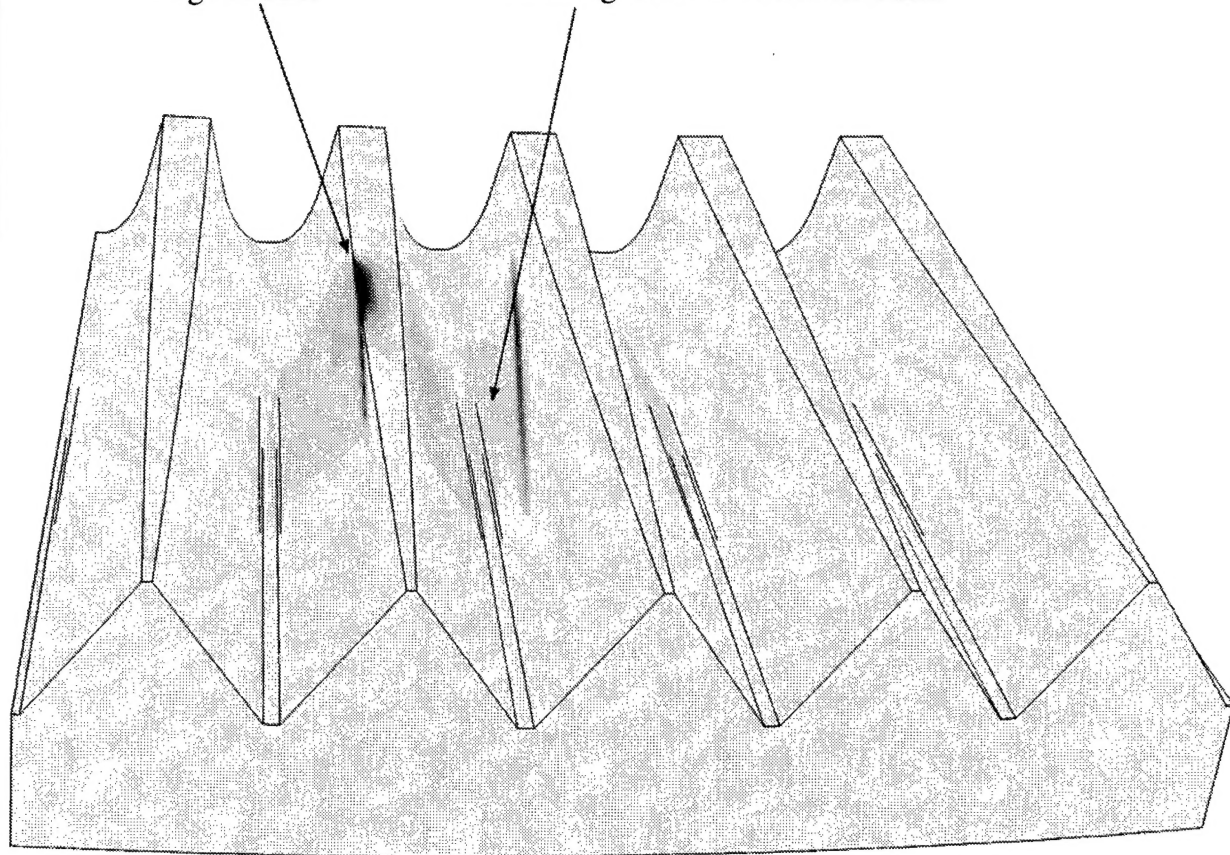
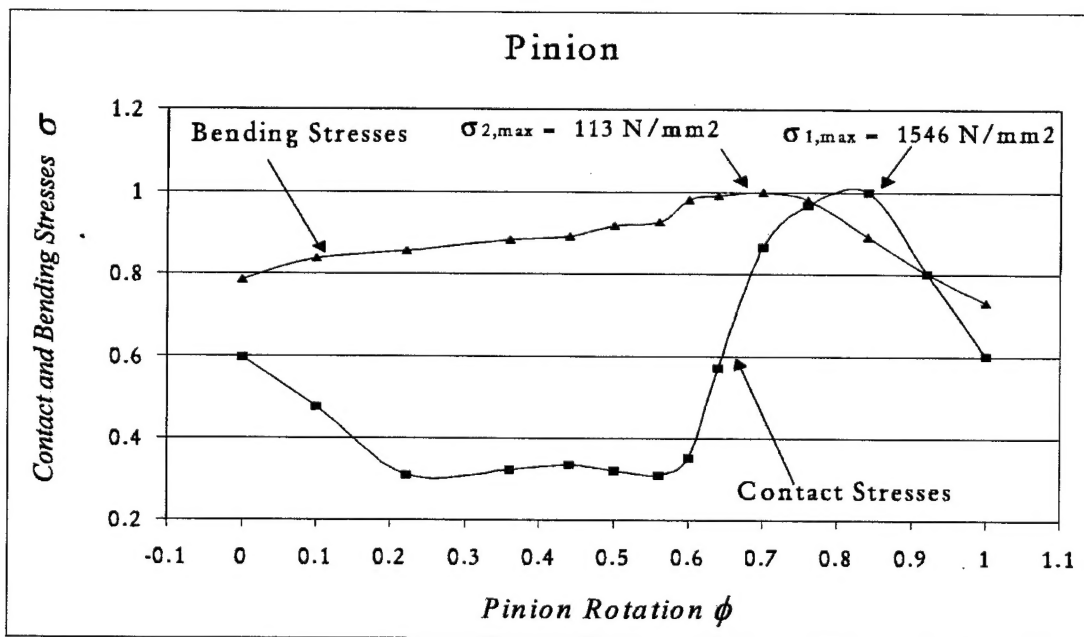Figure 24: Contact and bending stresses for version 1 of face-gear drive
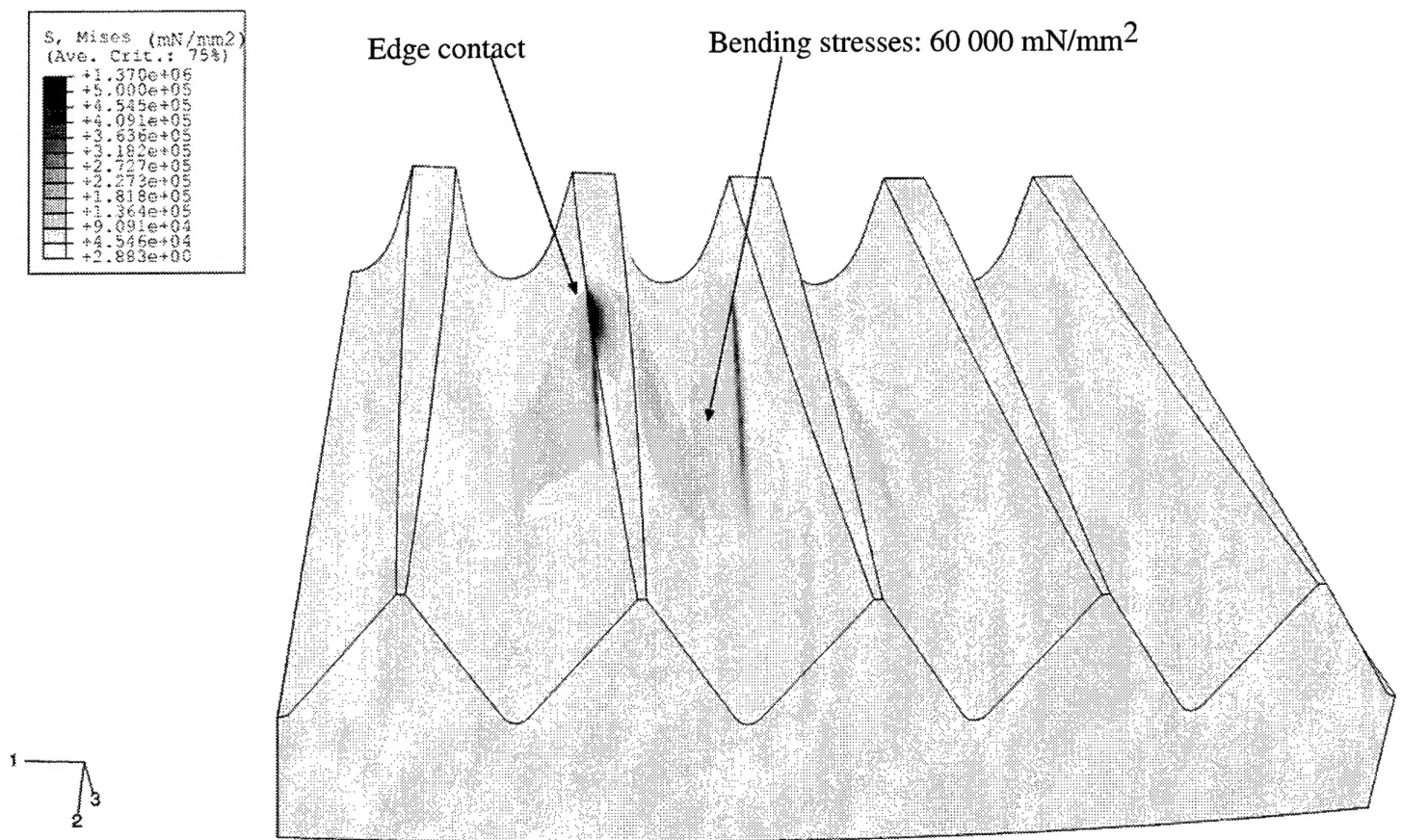
Figure 25: Contact and bending stresses for version 2 of face-gear drive
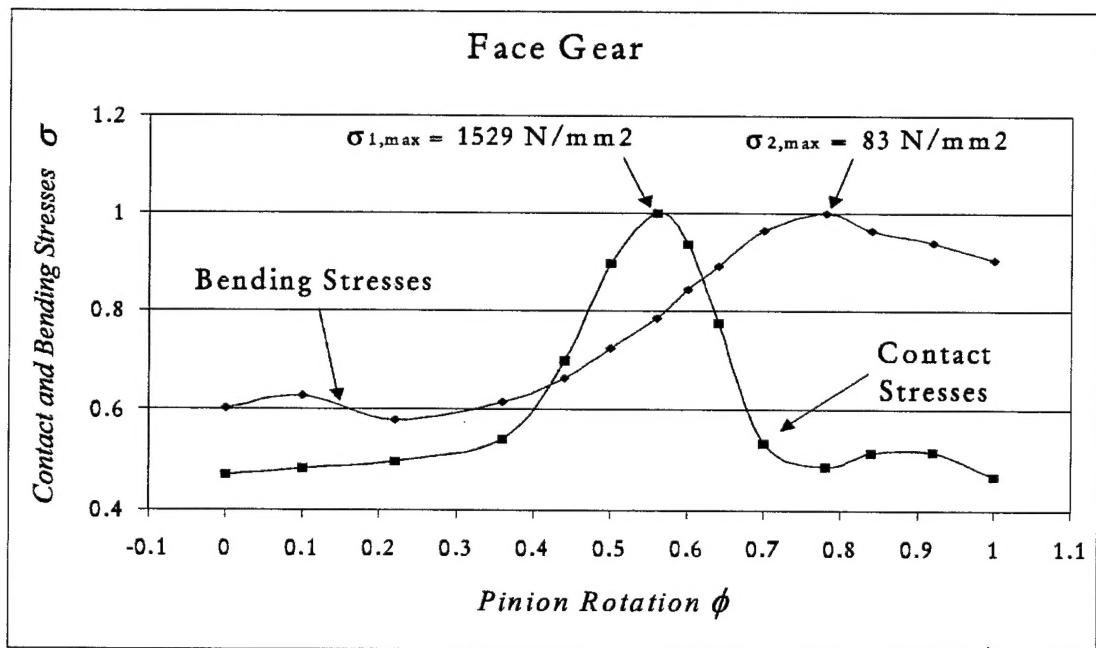
(a)

(b)

Figure 26: Variation of functions of contact and bending stresses during the cycle of meshing for (a) the face-gear and (b) the pinion

REPORT DOCUMENTATION PAGE

1. AGENCY USE ONLY (Leave blank)	2. REPORT DATE	3. REPORT TYPE AND DATES COVERED
	February 2002	Final Contractor Report

4. TITLE AND SUBTITLE

Face Gear Drive With Spur Involute Pinion: Geometry, Generation by a Worm, Stress Analysis

6. AUTHOR(S)

Faydor L. Litvin, Alfonso Fuentes, Claudio Zanzi, and Matteo Pontiggia

5. FUNDING NUMBERS

WU–728–30–10–00
NAG3–2450
1L162211A47A

7. PERFORMING ORGANIZATION NAME(S) AND ADDRESS(ES)

University of Illinois at Chicago
Gear Research Center
Department of Mechanical Engineering
Chicago, Illinois 60607

8. PERFORMING ORGANIZATION REPORT NUMBER

E–13183

9. SPONSORING/MONITORING AGENCY NAME(S) AND ADDRESS(ES)

National Aeronautics and Space Administration
Washington, DC 20546–0001
and
U.S. Army Research Laboratory
Adelphi, Maryland 20783–1145

10. SPONSORING/MONITORING AGENCY REPORT NUMBER

NASA CR—2002-211362
ARL–CR–491

11. SUPPLEMENTARY NOTES

Project Manager, Robert F. Handschuh, U.S. Army Research Laboratory, NASA Glenn Research Center, 216–433–3969.

12a. DISTRIBUTION/AVAILABILITY STATEMENT

Unclassified - Unlimited
Subject Category: 37   Distribution: Nonstandard

Available electronically at http://gltrs.grc.nasa.gov/GLTRS

This publication is available from the NASA Center for AeroSpace Information, 301–621–0390.

12b. DISTRIBUTION CODE

13. ABSTRACT (Maximum 200 words)

A face gear drive with a spur involute pinion is considered. The generation of the face gear is based on application of a grinding or cutting worm whereas the conventional method of generation is based on application of an involute shaper. An analytical approach for determination of: (i) the worm thread surface, (ii) avoidance of singularities of the worm thread surface, (iii) dressing of the worm, and (iv) determination of stresses of the face-gear drive, is proposed. A computer program for simulation of meshing and contact of the pinion and face-gear has been developed. Correction of machine-tool settings is proposed for reduction of the shift of the bearing contact caused by misalignment. An automatic development of the model of five contacting teeth has been proposed for stress analysis. Numerical examples for illustration of the developed theory are provided.

14. SUBJECT TERMS

Gears; Transmissions

15. NUMBER OF PAGES

50

16. PRICE CODE

17. SECURITY CLASSIFICATION OF REPORT	18. SECURITY CLASSIFICATION OF THIS PAGE	19. SECURITY CLASSIFICATION OF ABSTRACT	20. LIMITATION OF ABSTRACT
Unclassified	Unclassified	Unclassified	